Restoring synapse integrity and memory in Alzheimer's disease by downregulation of the Wnt antagonist Dickkopf-3

AUTHORS

Nuria Martin-Flores[1,4], Marina Podpolny[1,4], Faye McLeod[1], Karen Crawford[2], Dobril Ivanov[2], Valentina Escott-Price[2,3], Patricia C. Salinas[1*]

[1] Department of Cell and Developmental Biology, Division of Biosciences, University College London, UK

[2] Division of Psychological Medicine and Clinical Neurosciences, Cardiff University, UK

[3] UK Dementia Research Institute, Cardiff University, UK

[4] These authors contributed equally

* Correspondence should be addressed to:

Professor Patricia C. Salinas, p.salinas@ucl.ac.uk

ABSTRACT

Increasing evidence supports a role of deficient Wnt signaling in Alzheimer's disease (AD). Recent studies reveal that the secreted Wnt antagonist Dickkopf-3 (DKK3) is elevated in the human AD brain. Here, we investigate the contribution of DKK3 to synapse integrity in the healthy and AD brain. We uncover a novel genetic link between *DKK3* gene variants and AD risk. Our findings show that DKK3 protein is increased in different human brain fractions consistent with disease progression. In the hAPP-J20 and hAPP$^{NL\text{-}G\text{-}F/NL\text{-}G\text{-}F}$ AD models, DKK3 accumulates at plaques in the brain. Oligomers of amyloid-β enhance the secretion of DKK3 from cultured neurons and DKK3 secretion is also increased in hippocampal slices of hAPP-J20 mice. In addition, gain-of-function experiments revealed that DKK3 decreases the density of excitatory synapses through inhibition of the canonical Wnt/GSK3β pathway but increases inhibitory synapse density through activation of the Wnt/JNK pathway. Our studies demonstrate that *in vivo* DKK3 downregulation restores synapse number in hAPP-J20 mice. Importantly, DKK3 knockdown improves memory in this AD model. Collectively, our findings identify DKK3 as a novel driver of synapse defects and memory impairment in AD.

KEYWORDS

Alzheimer's disease, Wnt signaling, Dickkopf, synapse, synapse degeneration, memory, hAPP-J20, hAPP$^{NL\text{-}G\text{-}F/NL\text{-}G\text{-}F}$

INTRODUCTION

Alzheimer's disease (AD) is the most common form of dementia in the aging population. The disease is characterized by progressive synapse dysfunction and loss that precede neuronal death and the onset of clinical symptomatology. Indeed, synapse loss is an early signature that correlates with cognitive decline in AD (Mucke & Selkoe 2012; Selkoe & Hardy 2016). Current AD models suggest that amyloid-β (Aβ) initiates a pathophysiological cascade leading to synapse failure and eventually cognitive decline. Although deposition of Aβ into amyloid plaques is one of the main neuropathological hallmarks of AD together with neurofibrillary tangles, soluble Aβ oligomers (Aβo) are considered one of the key toxic proteins driving synapse dysfunction (Walsh et al. 2002; Mucke & Selkoe 2012; Selkoe & Hardy 2016). However, the exact mechanisms by which Aβo impair synapse function and cause degeneration are not fully understood.

Increasing evidence suggests that Wnt signaling is compromised in AD, contributing to synapse degeneration. Wnt secreted proteins play a crucial role in synapse formation, synaptic plasticity, and synapse integrity in the adult brain (McLeod & Salinas 2018). The canonical Wnt pathway is activated when Wnt ligands bind to Frizzled (Fz) receptors and the co-receptor low-density lipoprotein receptor-related protein 6 (LRP6), resulting in the inhibition of the serine/threonine kinase GSK3β and stabilization of β-catenin, triggering changes in gene expression and cytoskeletal dynamics (Niehrs 2012; Nusse & Clevers 2017). Evidence that the canonical Wnt pathway is impaired in AD comes from several findings. First, the level of Dickkopf-1 (DKK1), a secreted Wnt antagonist, is increased in the brain of AD patients and AD models (Caricasole et al. 2004; Rosi et al. 2010; Purro et al. 2012). Moreover, DKK1 promotes synapse degeneration and its blockade protects against Aβ-induced dendritic spine and synapse loss (Purro et al. 2012; Sellers et al. 2018). Second, downregulation of Kremen-1, a co-receptor for DKK1, protects synapses from Aβ toxicity (Ross et al. 2018). Third, the Wnt receptors Fz1 and Fz7 are downregulated in the hippocampus of $hAPP^{NL\text{-}G\text{-}F/NL\text{-}G\text{-}F}$ mice and human AD brain (Palomer et al. 2022). Fourth, three genetic variants in *LRP6* have been linked to late-onset AD, two of which confer decreased Wnt signaling in cell lines (De Ferrari et al. 2007; Alarcón et al. 2013). Furthermore, loss-of-function of LRP6 exacerbates amyloid pathology in an AD mouse model (Liu et al. 2014). Fifth, GSK3β activity is elevated and β-catenin level is reduced in the human AD brain (Leroy et al. 2007). Thus, Wnt signaling is a potential therapeutic target for synapse protection in AD.

DKK3, a structurally divergent member of the Wnt antagonist DKK family (Krupnik et al. 1999; Niehrs 2006), is emerging as a potential contributor to AD pathogenesis. Although

studies suggest that DKK3 antagonizes the Wnt canonical pathway (Caricasole et al. 2003; Mizobuchi et al. 2008; Zhu et al. 2014), the function of DKK3 in the adult brain is unclear. *DKK3* knock-out mice are viable and do not exhibit neurological alterations, except for hyperlocomotion in females (Barrantes et al. 2006). Recent findings indicate that DKK3 is upregulated in plasma, cerebrospinal fluid (CSF), and in the brains of AD patients (Zenzmaier et al. 2009; Bruggink et al. 2015; Hesse et al. 2019; Xu et al. 2019). Moreover, DKK3 accumulates in Aβ plaques in the human AD brain (Bruggink et al. 2015; Drummond et al. 2017; Xiong et al. 2019). Despite these findings, the impact of DKK3 on synapse and cognitive deficits in AD remains to be determined.

Here, we investigated the role of DKK3 in synapse integrity in the healthy and AD adult brain. Using human brain samples, we show that DKK3 expression is elevated in AD, coinciding with increased DKK3 protein in the soluble fraction of Braak stages I-III AD patients and the insoluble fraction of Braak stages IV-VI AD patients. Consistently, DKK3 secretion is increased in the hippocampus of an AD mouse model, before plaque deposition, and then accumulates in dystrophic neuronal processes around amyloid plaques at later stages. Our gain-of-function experiments uncover a novel role for DKK3 in triggering the loss of excitatory synapses with the concomitant increase in inhibitory synapses in the hippocampus. Importantly, *in vivo* DKK3 loss-of-function restores synapse number in the hippocampus and rescued memory in an AD mouse model. We further strengthened our findings by demonstrating a novel genetic association of *DKK3* with AD risk. Our studies identified DKK3 as a driver of synapse pathology and cognitive impairment in AD.

RESULTS

DKK3 is increased in the human AD brain

Studies using brain samples from AD patients revealed that DKK3 protein is increased in specific areas affected in AD (Hesse et al. 2019; Xu et al. 2019). To explore whether changes in protein levels correlate with gene expression, we examined levels of *DKK3* mRNA in the brain of AD patients using RNA-seq data from ROSMAP (De Jager et al. 2018), MSBB (Wang et al. 2018), and MayoRNAseq (Allen et al. 2016) (n = 248 controls, 379 AD cases) datasets. Logistic regression analyses revealed that *DKK3* was upregulated in AD cases (regression β-coefficient = 0.31; p-value = 1.52×10^{-3}). In addition, ordinal regression analyses showed that *DKK3* was differentially expressed in relation to Braak scores (Braak et al. 2006) (regression β-coefficient = 0.27; p-value = 8.84×10^{-4}) but not to CERAD scores (Mirra et al. 1991) (regression beta coefficient: 0.07; p-value = 0.43) (**Figure 1A**). We next assessed DKK3 protein levels in the hippocampus

of AD patients at different disease stages based on their Braak status. We evaluated healthy, Braak stages I-III and Braak stages IV-VI individuals (n = 16 per group, **Table S1**). Given that DKK3 is found at Aβ plaques in human AD brain (Bruggink et al. 2015; Drummond et al. 2017), we analyzed DKK3 protein from soluble and insoluble fractions of hippocampal homogenates. Soluble DKK3 levels were increased in Braak I-III patients when compared to control subjects (1.4-fold increase), but no changes were observed in Braak IV-VI (**Figure 1B**). In the insoluble fraction, in contrast, DKK3 protein levels were increased in Braak IV-VI (1.51-fold increase), but not in Braak I-III subjects (**Figure 1C**). These results demonstrate that *DKK3* mRNA and DKK3 protein levels are elevated in the brain of AD patients. Moreover, DKK3 protein increases early in AD in the soluble fraction but as the disease progresses this protein localizes to the insoluble fraction, which likely contains Aβ plaques.

DKK3 accumulates at atrophic neurites around amyloid plaques in AD mouse models

We next analyzed the exact location of DKK3 in the healthy and AD mouse hippocampus. In the mouse, DKK3 is expressed in excitatory neurons in different brain areas including the hippocampus and neocortex (Barrantes et al. 2006; Thompson et al. 2008; Meister et al. 2015). To study DKK3 expression, we used a specific DKK3 antibody, validated with brain samples isolated from *Dkk3*$^{-/-}$ mice by western blot (**Figure S1A**) and confocal microscopy (**Figure S1B**). In the mouse hippocampus, DKK3 protein was highly expressed in neurons of the CA1, CA2, and CA3 pyramidal layers but not in the dentate gyrus (DG) granule cell layer (**Figure S1C**) as previously reported (Barrantes et al. 2006; Thompson et al. 2008). In addition, DKK3 protein was present at lower levels in GFAP-positive cells (astrocytes) (**Figure S1D**), but not in IBA1-positive cells (microglia) (**Figure S1E**). Thus, principal neurons are the main source of DKK3 protein followed by astrocytes in the adult mouse hippocampus.

To further understand the role of DKK3 in the AD brain, we evaluated its localization within the hippocampus of two AD mouse models when Aβ plaques are present. Aβ plaques are complex structures closely associated with atrophic axons and dendrites of nearby neurons and glial cells (**Figure 2A**). Using confocal microscopy, we examined the presence of DKK3 in hippocampal Aβ plaques, detected using anti-Aβ (6E10), in 18-months old J20 (Mucke, Masliah, et al. 2000) and 8-months old NLGF mice (Saito et al. 2014). DKK3 was present at Aβ plaques in both AD lines (**Figure 2B**). Further characterization of J20 mice showed that DKK3 was present in 70% of Aβ plaques, visualized using ThioS (**Figure 2C**). This localization was specific for DKK3, as other

secreted proteins such as Wnt7a/b did not localize to Aβ plaques (**Figure S2A**). Furthermore, DKK3 was absent from astrocytes and microglia in the plaques but specifically colocalized with Neurofilament-H, indicating that DKK3 is present in atrophic neurites around amyloid plaques (**Figure 2D & Figure S2B&C**).

Secretion of DKK3 by Aβo and in AD mouse models requires NMDAR activation

The accumulation of DKK3 in Aβ plaques in AD led us to investigate whether Aβo affect DKK3 protein levels. Indeed, Aβo increased DKK3 protein levels by 2-fold in both the cellular lysate and the extracellular fraction of cultured hippocampal neurons (**Figure 2E and Figure S3A&B**), suggesting that Aβo did not only upregulate DKK3 protein levels but also enhanced its secretion. We next examined total and secreted levels of DKK3 from acute hippocampal slices of WT and J20 mice at 3-4 months, before plaques appear. Although the total DKK3 levels did not differ between J20 and WT mice in the homogenate, secreted DKK3 levels were significantly increased (2.54-fold increase) in J20 mice (**Figure 2F**).

Our next studies focused on understanding the mechanisms underlying increased secretion of DKK3 in J20 mice. Mounting evidence demonstrates that Aβo trigger the overactivation of *N*-methyl-D-aspartate (NMDA) receptors (NMDARs), which contributes to long-term depression (LTD) in AD models (Li et al. 2011; Mucke & Selkoe 2012). We, therefore, investigated the contribution of NMDARs by blocking them with (2R)-amino-5-phosphonovaleric acid (APV). APV completely prevented DKK3-enhanced secretion in J20 brain slices (**Figure 2F**). Next, we examined whether DKK3 was regulated by NMDAR-mediated synaptic plasticity by inducing chemical long-term potentiation (cLTP) or chemical long-term depression (cLTD) in cultured hippocampal neurons. Induction of cLTP did not affect DKK3 protein levels in the cellular or extracellular fractions (**Figure S3C**). In contrast, cLTD significantly increased the secretion of DKK3 without affecting its cellular levels (**Figure S3D**). Similar results were obtained in brain slices following cLTD induction (**Figure S3E**). Moreover, the exocytosis inhibitor brefeldin A (BFA) reduced DKK3 release in control conditions and completely blocked cLTD-induced DKK3 release (**Figure S3E**). Our results suggest that DKK3 secretion is enhanced in AD through NMDAR-mediated LTD.

DKK3 differentially affects excitatory and inhibitory synapses in the adult hippocampus

Given that the Wnt antagonist DKK1 leads to excitatory synapse disassembly and synaptic plasticity defects (Galli et al. 2014; Marzo et al. 2016; Galli et al. 2021), we evaluated the impact of increased levels of DKK3 on synapses by performing *ex vivo*

gain-of-function experiments (**Figure 3A**). We focused on the CA3 region as DKK3 is highly expressed in this hippocampal region (Thompson et al. 2008) and it is also required for encoding spatial and other episodic memories, which are impaired in AD (Deuker et al. 2014). Moreover, we previously reported that Aβo trigger synapses loss in the CA3 *stratum radiatum* (SR) region of the hippocampus (Purro et al. 2012). Gain-of-function of DKK3 reduced the puncta number of the excitatory presynaptic marker vGLUT1 (by 38.99%), the postsynaptic marker PSD-95 (by 32.58%) and the total number of excitatory synapses (by 60.85%), determined by the colocalization of these synaptic markers, in the CA3 SR (**Figure 3B**). These changes in synapse number were not due to neuronal death (**Figure S4A&B**). Patch-clamp recordings of CA3 neurons revealed that DKK3 gain-of-function decreased the frequency of miniature excitatory postsynaptic currents (mEPSC) by 48.54% but did not affect the amplitude (**Figure 3C**).

We further investigated whether DKK3 gain-of-function affects inhibitory synapses. Notably, DKK3 increased the density of puncta for the inhibitory postsynaptic marker gephyrin (by 55.39%) without affecting the density of the inhibitory presynaptic marker vGAT in the CA3 SR (**Figure 3D**). Consistently, DKK3 increased the number of inhibitory synapses (by 65.99%) (**Figure 3D**). Patch-clamp recordings of CA3 neurons uncovered that DKK3 increased the frequency of miniature inhibitory postsynaptic currents (mIPSC) by 65.56% but did not affect the amplitude (**Figure 3E**). In the CA1 SR, DKK3 induced similar effects on excitatory and inhibitory synapse density (**Figure S4C&D**). Together, these results demonstrate that DKK3 gain-of-function decreases excitatory synapse number but increases inhibitory synapse number in the adult hippocampus.

DKK3 regulates excitatory and inhibitory synapse density through different Wnt signaling pathways

We next examined the Wnt signaling pathways mediating DKK3-induced synaptic changes. Wnts can signal through different pathways, including the Wnt/GSK3 and Wnt/JNK cascades (**Figure 4A**) (Niehrs 2012; Nusse & Clevers 2017). A previous study showed that Dkk1 induces synapse loss by blocking canonical Wnt pathway in the hippocampus (Marzo et al. 2016). To investigate if DKK3 triggers synaptic changes through this pathway, we evaluated the puncta density of β-catenin, which is degraded upon inhibition of Wnt/GSK3β signaling (Nusse & Clevers 2017). To exclude changes in β-catenin density due to synapse loss, we measured the density of extra-synaptic β-catenin as we had done before (Galli et al. 2014). Indeed, DKK3 decreased extra-synaptic β-catenin puncta number in hippocampal slices (**Figure 4B**). To further explore the role of the Wnt/GSK3β cascade, we activated this pathway using the GSK3 inhibitor

6-bromoindirubin-3'-oxime (BIO) (Zhang et al. 2015; Marzo et al. 2016) in brain slices. At the concentration used, BIO did not promote the assembly of excitatory synapses in control conditions, but completely blocked DKK3-induced loss of excitatory synapses (**Figure 4C**). Similar results were obtained with CHIR99021, another highly specific GSK3 inhibitor (Ring et al. 2003) (**Figure S4E**). Thus, DKK3 affects excitatory synapse number through the canonical Wnt pathway.

Next, we investigated if DKK3 increases inhibitory synapses through the canonical Wnt signaling pathway by blocking GSK3 using BIO. In contrast to excitatory synapses, BIO did not prevent DKK3's impact on inhibitory synapse density (**Figure S4F**). Therefore, DKK3 affects inhibitory synapse density independent of the Wnt/GSK3 pathway. Previous studies showed that Dkk1, member of the Dkk family, concomitantly inhibits the Wnt/GSK3β pathway and activates the Wnt/ Planar Cell Polarity (PCP) signaling cascade (Caneparo et al. 2007; Killick et al. 2014; Marzo et al. 2016). The PCP pathway activates c-Jun N-terminal kinase (JNK), which has been implicated in Aβ toxicity (Killick et al. 2014). We, therefore, tested the Wnt/JNK pathway by using CC-930, a JNK inhibitor (Krenitsky et al., 2012). CC-930 blocked DKK3-induced elevation of gephyrin puncta number and inhibitory synapse density (**Figure 4D**). Together, our results indicate that DKK3 induces the loss of excitatory synapses through inhibition of Wnt/GSK3β signaling but increases inhibitory synapses through activation of the Wnt/JNK pathway.

In vivo DKK3 loss-of-function decreases inhibitory synapses without affecting excitatory synapses

We next studied the *in vivo* role of DKK3 by downregulating DKK3 in adult WT mice using a viral transduction approach. DKK3 was knocked down in the CA3 region of the hippocampus using AAV9 expressing enhanced green fluorescent protein (EGFP) and scramble shRNA (Scr shRNA) or shRNA against DKK3 (DKK3 shRNA) (**Figure 5A**), and synapses were evaluated one month later. We validated the *in vivo* knockdown of DKK3 expression, which was approximately 85% at the injection site (**Figure 5A**). Excitatory and inhibitory synapses were assessed by confocal microscopy and by whole-cell patch-clamp recordings. In contrast to gain-of-function experiments, DKK3 silencing did not affect excitatory synapse number (**Figure 5B**) or mEPSC frequency (**Figure 5C**). However, DKK3 loss-of-function decreased the amplitude of mEPSCs by 28.18% (**Figure 5C**). Conversely, knockdown of DKK3 reduced the number of inhibitory synapses (by 37.30%, **Figure 5D**), the frequency (by 71.76%), and amplitude of mIPSCs (by 35.02%) (**Figure 5E**). Thus, downregulation of DKK3 in the healthy adult brain reduces the number of inhibitory synapses.

In vivo DKK3 loss-of-function restores excitatory and inhibitory synapse changes in J20 mice

To investigate the contribution of DKK3 to synaptic changes in AD, we knocked down DKK3 in the hippocampus of J20 mice at two different disease stages using AAV9-Scr shRNA or AAV9-DKK3 shRNA. J20 mice exhibit excitatory synapse loss in the hippocampus at 4-months of age (early stage), whereas plaque deposition starts around 5-months, and is widely distributed in the cortex and hippocampus by 9-months (late stage) (Mucke, Masliah, et al. 2000; Mucke, Yu, et al. 2000; Meilandt et al. 2009; Hong et al. 2016). We first evaluated the contribution of DKK3 to excitatory and inhibitory synapses in J20 mice at early stages (**Figure 6A & Figure S5A**). As previously reported, 4-months old J20 mice exhibited a 40-45% loss of excitatory synapses in the CA3 SR when compared to WT (Hong et al. 2016). Remarkably, DKK3 knockdown restored excitatory synapse number in J20 mice (**Figure 6B & Figure S5B**). Next, we examined inhibitory synapses and found an increase of 20.60% in J20 mice compared to WT (**Figure 6C**). Importantly, DKK3 silencing also rescued inhibitory synapse number in these mice (**Figure 6C** and **Figure S5C**). Thus, *in vivo* DKK3 loss-of-function restores synapse number in J20 mice, supporting the hypothesis that DKK3 is a key contributor to synaptic changes in this mouse model.

A key feature of AD brains is loss of synapses around Aβ plaques (Koffie et al. 2012). Therefore, we investigated whether DKK3 affects synapse number around plaques in 9-months old J20 mice. We observed a significant effect of distance on the density of excitatory from the core of the plaque ($F(6, 318) = 27.26$, p-value < 0.0001) and inhibitory synapses ($F(6, 276) = 23.51$, p-value < 0.0001) (**Figure 6D&E**). Importantly, DKK3 silencing significantly increased the number of excitatory synapses (**Figure 6D & Figure S5D**) but decreased the density of inhibitory synapses around plaques (**Figure 6E & Figure S5E**) when compared to J20 mice injected with Scr shRNA. These results demonstrate that loss-of-function of DKK3 ameliorates excitatory and inhibitory synapse changes in J20 mice at two stages, before plaque burden starts (4-months old), and later when amyloid plaque pathology is evident (9-months old).

In vivo DKK3 loss-of-function improves memory function in J20 mice

The finding that DKK3 loss-of-function reverses synaptic changes at early and late stages in the J20 mice led us to test whether silencing DKK3 restores hippocampal-mediated learning and memory in these mice (**Figure 7A**). Knockdown of DKK3 using viral injections did not affect exploratory activity or anxiety in J20 mice (**Figure S6A&B**). In contrast, DKK3 downregulation significantly improved spatial memory in J20 mice as

evaluated by the novel object location test (NOLT) (**Figure 7B**). Next, we examined long-term spatial working memory using the Morris Water Maze (MWM). No deficiencies in vision or locomotion were observed as escape latencies did not differ between groups when the platform was visible (**Figure S6C**). We also assessed reference spatial learning using the hidden platform version of the MWM (**Figure 7C**). Performance improved significantly in all 4 groups during training, although the escape latency in J20-Scr shRNA mice remained significantly higher than WT-Scr shRNA mice (**Figure 7C**). Importantly, silencing DKK3 in J20 mice fully rescued this defect (**Figure 7C**). To test spatial memory, probe trials were performed on day 5 (early probe) and day 8 (late probe). In the first early probe test, J20-Scr shRNA animals traveled significantly less in the target quadrant than WT-Scr shRNA mice (**Figure 7D**). After further training, in the late probe, the time to first entrance to the target location (platform) and the distance traveled in the target quadrant were rescued in the J20-DKK3 shRNA mice when compared to J20-Scr shRNA mice (**Figure 7E**). Together, these results demonstrate that DKK3 downregulation in the hippocampus restores cognitive function in J20 AD mice.

DKK3 gene is associated with increased risk of AD

Our findings in AD patients (**Figure 1**) and AD mouse models (**Figures 2, 6 & 7**) suggest that increased levels of DKK3 drive synaptic changes and memory impairment in AD. This led us to test whether there is a genetic association between *DKK3* and late-onset AD risk. We therefore examined data obtained from a genome-wide association study (Kunkle et al. 2019). We found 33 SNPs in the *DKK3* gene that reached a nominal significance, with a p-value of 0.003 in the most significantly associated SNP (rs11602449) (**Figure 8A & Table S2**). To account for the number of SNPs in the gene and linkage disequilibrium (LD) between them, we performed a gene-based analysis. This analysis also showed a significance association of *DKK3* gene with AD (p-value = 0.008). In summary, this novel identification of a genetic link between *DKK3* and AD together with our findings in human AD brain and our functional studies in mice strongly support a role for DKK3 in synapse dysfunction and memory impairment in AD (**Figure 8B**).

DISCUSSION

In AD, synapse loss is the strongest correlate with cognitive impairment (Mucke & Selkoe 2012; Selkoe & Hardy 2016). However, the mechanisms that trigger synaptic changes remain poorly understood. In this work, we investigated the function of the Wnt antagonist DKK3 on synapse integrity and memory in the healthy and AD brain. Our functional analyses in AD models and our studies in humans strongly support the notion

that DKK3 contributes to synapse defects and memory impairment in AD. Importantly, we identified a novel genetic link between *DKK3* and late-onset AD.

DKK3 was originally identified as a structurally divergent member of the DKK family of secreted Wnt antagonists (Krupnik et al. 1999). Although DKK3 is the DKK member most highly expressed in the human and mouse brain (Zhang et al. 2014), its function in this tissue has remained unknown. Here we demonstrate a novel role for DKK3 in differentially regulating both excitatory and inhibitory synapses in the hippocampus. Indeed, gain-of-function of DKK3 decreases the number of excitatory synapses but increases inhibitory synapses in the adult hippocampus. Conversely, *in vivo* knockdown of endogenous DKK3 in adult WT mice decreases inhibitory synapses but does not affect excitatory synapse density. However, knockdown of DKK3 reduces the amplitude of mESPCs. A possible explanation for this finding is that DKK3 affects the function of excitatory synapses in WT mice without affecting their structural stability. Our results also demonstrate that DKK3 signals through different pathways to regulate excitatory and inhibitory synapses. Activation of the canonical Wnt pathway by inhibition of GSK3 blocks DKK3-mediated excitatory synapse loss, which is consistent with a role of DKK3 as an antagonist of canonical Wnt signaling (Caricasole et al. 2003; Mizobuchi et al. 2008; Zhu et al. 2014). In contrast, blockade of GSK3 does not restore DKK3 impact on inhibitory synapse number. Instead, JNK blockade prevents DKK3-induced inhibitory synapse assembly, indicating a role for Wnt/JNK signaling in this process. In line with these results, studies showed that DKK3 activates JNK (Abarzua et al. 2005; Mizobuchi et al. 2008; Yu et al. 2017). Together, our results indicate that DKK3 regulates the stability of excitatory and inhibitory synapses in the adult hippocampus. These results are in contrast to those described for another member of this family of Wnt antagonist, DKK1, which only affects excitatory synapses in the mouse hippocampus and inhibitory ones are spared (Marzo et al. 2016). These suggest that receptors for DKK3 and DKK1 might be different in different neurons.

A previous work revealed that DKK3 is present at Aβ plaques in the brain of AD subjects (Bruggink et al. 2015), which was later confirmed by other proteomic studies in human and mouse brains (Drummond et al. 2017; Xiong et al. 2019). In agreement with these findings, we demonstrate that DKK3 accumulates at Aβ plaques in two AD mouse models, the NLGF and J20 lines. We found that DKK3 specifically localizes to dystrophic neurites surrounding the plaques. Proteomic studies also showed increased levels of DKK3 in brain-affected areas, including the hippocampus and cortical synaptosomes of AD patients (Hesse et al. 2019; Xu et al. 2019). Consistently, our results demonstrate an upregulation of DKK3 at the mRNA and protein levels in human AD brain samples.

Importantly, DKK3 upregulation starts early in AD, as we observe increased DKK3 protein levels in Braak I-III subjects. In contrast to these studies and our findings, a work reported reduced levels of DKK3 in human AD brain and in an AD mouse model (Zhang et al. 2017) but the specificity of the DKK3 antibody was not demonstrated. Our analyses using a validated antibody revealed that DKK3 is not present in granular neurons in the hippocampus as other works reported (Barrantes et al. 2006; Thompson et al. 2008) and that it is elevated in the brain from AD patients. Moreover, the authors indicated that overexpression of DKK3 restored memory in an AD model. However, the generation of these mice were not fully characterized (Zhang et al. 2017). In conclusion, our results are consistent with several other findings that DKK3 levels are increased in AD.

Several studies showed that Aβo block glutamate uptake by neurons, raising the extracellular glutamate levels and aberrantly activating NMDARs, leading to impaired synaptic function and memory (Li et al. 2011; Mucke & Selkoe 2012). Furthermore, blockade of NMDARs preserves synapse density and cognitive function in AD mouse models (Ye et al. 2004; Hu et al. 2009). Our studies revealed that acute exposure to Aβo increase total and secreted DKK3 levels in neurons. Moreover, increased DKK3 secretion in the hippocampus of J20 mice is completely abolished by blockade of NMDARs. Conversely, DKK3 secretion is increased by NMDAR-induced cLTD, suggesting that overactivation of NMDARs triggers DKK3 release. These results provide mechanistic insights into how DKK3 secretion is increased in AD. Concomitant with changes in DKK3 levels, we demonstrate that knocking down DKK3 in J20 mice restores excitatory and inhibitory synaptic numbers in the hippocampus. Crucially, downregulation of DKK3 also improves cognitive function, particularly spatial memory, in J20 mice. Based on these findings, we propose that Aβo promote LTD induction triggering DKK3 release, which in turn impairs synapse integrity and function resulting in memory deficits in AD.

Our genetic studies also uncover for the first time that the *DKK3* gene is linked to late-onset AD. AD is a complex polygenic and multifactorial disease. To date, variants in the Wnt co-receptor *LRP6* are the only genetic associations linking Wnt signaling to late-onset AD (De Ferrari et al. 2007; Alarcón et al. 2013). Our SNP- and gene-based analyses identified a novel genetic link between *DKK3* and late-onset AD, strengthening the role of deficient Wnt pathway in AD. Among the SNPs in *DKK3*, rs11602449 (C/T) is the most significantly associated with AD. This SNP is located in an intronic region, with a minor allele frequency of 0.25 in the European population and 0.22 in the global population (1000 Genomes Project Consortium et al. 2015). Nevertheless, this SNP might be in linkage disequilibrium with other functional variants that could also affect

DKK3 gene expression or protein stability. Although we found a moderate genetic link, our results using human AD brain samples and AD mouse models give strong support for a contribution of DKK3 in AD pathogenesis. Together, our findings provide functional and genetic evidence for a novel role of DKK3 in synaptic and cognitive changes in AD. Our studies also identify DKK3 as a potential target for ameliorating synapse degeneration and memory impairment in AD.

SUPPLEMENTARY INFORMATION

For further information see Supplementary Figures and Tables.

ACKNOWLEDGEMENTS

We would like to thank Professors Takashi Saito and Takaomi Saido for the APP^{NL-G-F} mice and Professors Qingbo Xu for providing us brain samples of the *DKK3* KO mice. We thank members of the Salinas lab and our collaborators Professors Francesca Cacucci and Alasdair Gibb for their support and discussion on this project. We also thank Dr Ganna Leonenko for her assistance in genetic analyses. Diagrams included in the figures were created with Biorender.com. This work was funded by Alzheimer's Society (AS-PG-17-006), MRC (MR/S012125/1 and MR/M024083/1), Alzheimer's Research UK (ARUK-PG2018A-002).

AUTHOR CONTRIBUTIONS

N.M.-F., M.P. and P.C.S. contributed to the conception and design of the study and the interpretation of the results. M.P. and N.M.-F. generated and analyzed the results. F.M. conducted and analyzed patch-clamp recording experiments. K.C., D.I. and V.E.-P. performed human RNAseq and genetic studies. N.M.-F., M.P. and P.C.S. prepared the figures and wrote the manuscript. All authors reviewed and approved the final version of this manuscript.

DECLARATION OF INTERESTS

The authors declare no competing interests.

MATERIALS AND METHODS

Human tissue

Anonymized human samples from control and AD patients were obtained from Cambridge Brain Bank (CBB), Division of the Human Research Tissue Bank, Addenbrooke's Hospital, Cambridge, UK. All samples were obtained with informed consent under CBB license (NRES 10/HO308/56) approved by the NHS Research Ethics Services. Tissues were stored at -80°C. Demographic data and Braak stages for each subject are shown in **Supplementary Table 1**.

Human RNAseq analyses

The reprocessed ROSMAP (De Jager et al. 2018), MSBB (Wang et al. 2018) and MayoRNAseq (Allen et al. 2016) temporal cortex RNASeq datasets and their associated phenotypic data such as Braak (Braak et al. 2006) and CERAD (Mirra et al. 1991) scores were downloaded from the AMP-AD consortium (https://www.synapse.org/#!Synapse:syn2580853/wiki/409840). For the ROSMAP study, AD cases were defined as individuals with a cognitive diagnosis of AD with no other cause of cognitive impairment (cogdx = 4 and cogdx = 5), and controls defined as those with no cognitive impairment (cogdx = 1). For the MSBB dataset, controls were defined as those with a CERAD score of 1 (normal) and a clinical dementia rating (CDR) of 0 or 0.5 (no cognitive deficits or questionable dementia respectively), whereas cases were defined as subjects with CERAD score of 2, 3 or 4 (possible, probable, definite AD) and a CDR of 2 or greater (mild dementia, moderate dementia, or severe to terminal dementia). For the MayoRNASeq dataset, individuals were already classified as an AD case or control based on neuropathology. All cases had a Braak stage of IV or greater. Controls had a Braak stage of III or less.

RNASeq datasets underwent quality control using RNASeQC (DeLuca et al. 2012) and were normalized for gene length and GC content with lowly expressed genes filtered out. Following quality control and normalization, 16,485 genes remained in the analysis. Linear mixed effect models (LMEM) in combination with principal component (PC) analyses were performed on normalized counts to combine data and adjust for batch effects and hidden confounders. LMEM used sex, age at death and the first three principal components as fixed effects, whilst individual ID and sequencing batch were used as random effects. Logistic regression was then performed on residuals from the LMEM for AD case/control status (n = 379 AD cases, 248 controls). Ordinal regressions were also performed on residuals from the LMEM for Braak stage (0-6) (n = 627) and

CERAD scores (1-4) (n = 537). The β-coefficient indicates the degree of differential *DKK3* expression.

Human genetic association analyses

To look for evidence of genetic association of *DKK3* to AD we used the summary statistics from the largest clinically assessed case-control GWAS study on AD (n = 63,926) (Kunkle et al. 2019). This consisted of 21,982 AD cases and 41,944 controls. SNPs in the *DKK3* gene were extracted according to chr11:11984653-12031316, as in GRCh37/hg19, resulting in 211 SNPs, and LocusZoom lots of regional associations were created using LocusZoom (Boughton et al. 2021).

To account for the number of SNPs in the gene (n = 211) and the linkage disequilibrium (LD) between SNPs, we run gene-based analysis using a computationally efficient gene-based tool MAGMA v1.06 (de Leeuw et al. 2015) with gene-annotation file NCBI37.3.gene.loc and calculated the gene-based p-value for the *DKK3* gene using AD summary statistics (Kunkle et al. 2019). Given that we tested one hypothesis, namely the association of *DKK3* with AD risk, the genome-wide correction for multiple testing was not a requirement. We mapped a SNP to a gene (as defined by NCBI 37.3) if it resided within the gene boundaries. The LD between SNPs was estimated with the European reference panel in 1000 Genomes phase 3.

Primary hippocampal cultures and treatments

Primary hippocampal neurons (700 cells/mm^2) were isolated from embryonic day 18 Sprague-Dawley rat embryos and cultured on poly-L-lysine coated plates in Neurobasal medium containing N2 and B27 supplements (Invitrogen). Neurons were maintained in a 5% CO_2 humified atmosphere at 37ºC. One-third of the media was replenished every seven days. All experiments were performed at 20-21 days-in-vitro (DIV).

Aβ oligomers (Aβo) preparation

Aβo were prepared from a commercially available Aβ1-42 peptide (Bachem, 4014447) as previously described (Purro et al. 2012). Briefly, Aβ1-42 peptide was dissolved in ice-cold HFIP to 1 mM concentration and left for 1 hour to monomerize at room temperature. HFIP was then allowed to evaporate overnight, creating a transparent film of Aβ. The Aβ films were stored at -80°C until fresh Aβo preparation was required. For preparation of the Aβo, DMSO was added to dissolve the Aβ film (5 mM). The solution was then mixed by vortexing for 60 seconds. Sterile PBS or Neurobasal was then added to achieve a final Aβ concentration of 100 μM, and the peptide was left to oligomerize for 24 hours at 4°C. Undissolved peptide was removed by centrifugation for 10 minutes at 12,000rpm

and the solution was collected. Quality of the Aβo preparation was assessed by Western Blot or by negative staining in EM. 21DIV dissociated hippocampal neurons were treated with 1 μM Aβo (monomers, trimers and tetramers) or vehicle (0.02% DMSO in Neurobasal) for 3 hours at 37 °C.

Chemical LTP and chemical LTD

Hippocampal neurons were subjected to chemical long-term potentiation (cLTP) or chemical long-term depression (cLTD) at 21DIV. As previously described, cLTP was induced using glycine (McLeod et al. 2018) and cLTD was induced using NMDA (Kamal et al. 1999). Briefly, 200μM glycine (Fisher Chemical, 10070150) or 20μM NMDA (Tocris Bioscience, 0114) (or the vehicle PBS) were applied to cultures for 10 or 5 minutes respectively. The media was then replaced with fresh medium. After 45 minutes, neurons and extracellular media were processed for Western Blot analyses. Levels of phospho-GluA1 Ser845 and total GluA1 were evaluated as readout.

Mice

All procedures involving animals were conducted according to the Animals Scientific Procedures Act UK (1986) and in compliance with the ethical standards at University College London (UCL). WT C57BL/6J were obtained from Jackson Laboratories. J20 mice were obtained from Jackson Laboratories and maintained on a C57BL/6J genetic background. J20 hemizygous transgenic males were bred with WT C57BL/6J females to generate hemizygous transgenic mice (J20) and WT littermates. Genotyping was performed using DNA from ear biopsies and with the following primers to detect the human APP transgene: forward 5'- GGTGAGTTTGTAAGTGATGCC-3' and reverse 5'-TCTTCTTCTTCCACCTCAGC -3'. $APP^{NL\text{-}G\text{-}F/NL\text{-}G\text{-}F}$ mice were obtained from (Saito et al. 2014) and maintained in C57BL/6J background as previously described (Palomer et al. 2022). Animals were housed in ventilated cages with access to food and water ad libitum and kept at 22±2°C and 55±10% humidity with a 12h/12h light cycle. Experimental animals included males and females. The ages of mice are specified in each figure legend, according to the experimental approach used.

Hippocampal stereotactic surgery

Stereotactic injection of AAV9-EGFP-U6-Scramble shRNA or AAV9-EGFP-U6-DKK3 shRNA was performed bilaterally in the CA3 area of the hippocampus. AAVs were purchased from VectorLabs. The sequence for Scr shRNA and DKK3 shRNA were as follows: Scr shRNA, 5'-CCTA AGGTTAAGTCGCCCTCGCTCGAGCGAGGGCGACTTAACCTTAGGTTTTT-3' and

DKK3 shRNA, 5'-GAGCCATGAATGTATCATTGACTCG AGTCAATGATACATTCATGGCTCTTTTT-3'. Adult mice were deeply anesthetized using a mixture of oxygen and isoflurane (4% for induction and 2-1% for maintaining anesthesia). Using a stereotactic frame, two injections were performed in the hippocampus at the following coordinates relative to bregma [anteroposterior (AP) and mediolateral (ML) and to dural surface (dorsoventral (DV): (1) -1.7AP, ±2 ML, -1.85 DV; (2) -2.3 AP, ±2.8 ML, -2.2 DV. Viral particles were injected into the brain using a 10µl syringe (Hamilton, 65460-05) at an infusion rate of 100nl/min with a microinjection serynge pump (World Precision Instruments, UMP3 UltraMicroPump). The needle was left for 5 additional minutes to ensure diffusion of the virus, then slowly retracted from the brain. After 4 weeks, synapses or behavior were evaluated.

Treatment of acute hippocampal slices

WT and J20 brain mice were rapidly dissected and place in 5% CO_2/95% O_2 ice-cold aCSF containing (in mM): 87 NaCl, 2.5 KCL, 25 $NaHCO_3$, 1.25 Na_2HPO_4, 0.5 $CaCl_2$, 7 $MgCl_2$, 10 D-(+)-Glucose, 75 sucrose (pH = 7.4). Sagittal 300 µm slices were obtained with a vibratome (Leica, VT100S) and transferred to 5% CO_2/95% O_2 aCSF (34ºC) containing (in mM): 125 NaCl, 2.5 KCL, 25 $NaHCO_3$, 1.25 Na_2HPO_4, 1 $CaCl_2$, 2 $MgCl_2$, 25 D-(+)-Glucose (pH = 7.4). Brain slices were maintained in warm aCSF solution for 60 min before starting treatments.

Brain slices were treated with 150 ng/ml recombinant DKK3 (R&D, 1118-DK) or vehicle control (PBS) for 4h (for synapse density evaluation) or 200 ng/ml for 3h (for electrophysiological recordings). Drugs used include 0.5 µM BIO (Calbiochem, 361550) or vehicle (DMSO); 60 nM CC-930 (Cayman Chemicals, CAY22466) or vehicle (DMSO); 1µM CHIR99021 (Calbiochem, 361559) or vehicle (DMSO); 20 µM NMDA (Tocris Bioscience, 0114) or vehicle (PBS); 50 µM APV (Tocris Biosciences, 0106) or vehicle (PBS); 10 µg/ml Brefeldin A (Biolegend, 420601) or vehicle (DMSO).

Electrophysiology

Transverse hippocampal slices (300µm) were cut on vibratome (Leica, VT100S) in ice-cold aCSF bubbled with 95% O_2 /5% CO_2 containing (in mM): 125 NaCl, 2.4 KCl, 26 $NaHCO_3$, 1.4 NaH_2PO_4, 20 D-(+)-Glucose, 0.5 $CaCl_2$ and 3 $MgCl_2$ as previously described (Redlingshöfer et al. 2020). CA3 pyramidal were patched in whole cell voltage-clamp configuration using pipettes (resistance 5–8 MΩ) pulled from borosilicate glass (Harvard, GC150F-7.5) and filled with caesium gluconate intracellular solution containing (in mM): 130 D-gluconic acid lactone, 10 Hepes, 10 EGTA, 10 NaCl, 0.5 $CaCl_2$, 1 $MgCl_2$, 1 ATP and 0.5 GTP, 5 QX314 (pH to 7.2 with CsOH). Slices were perfused with the same

aCSF solution as before except substituted with 1mM $MgCl_2$ and 2mM $CaCl_2$. All miniature currents were recorded in the presence of 100nM Tetrodotoxin (TTX, Abcam, ab120055). mEPSCs were held at -60 mV with 10μM bicuculline (Tocris Biosciences, 0130) and 50 μM APV (Tocris Biosciences, 0106) added, whereas mIPSCs were held at 0 mV in the presence of 50 μM APV (Ciani et al. 2011). Currents were recorded using an Axopatch 200B amplifier (Molecular Devices) and low pass filtered at 1 kHz and digitized (10 kHz). Analyses were performed using a combination of WinEDR and WinWCP software. For event detection, the "template" function in WinEDR software was used (Clements & Bekkers 1997). Several filters were applied to exclude events that were unlikely to be genuine.

Tissue processing for immunofluorescence microscopy

Acute slices (300 μm) were fixed in 4% paraformaldehyde (PFA)/4% sucrose for 20 minutes. Brains used for obtaining cryosection slices were fixed overnight in 4% PFA followed by cryopreservation in 30% sucrose before freezing. Free-floating sagittal hippocampal sections (30 μm) were obtained using a cryostat (Leica, CM1850).

Immunofluorescence staining of brain slices was performed as previously described (Marzo et al. 2016; McLeod et al. 2018). Briefly, slices were permeabilized and blocked using 10% donkey serum and 0.3% (for cryosections) or 0.5% (for acute slices) Triton X-100 in PBS for 3-5 hours at room temperature. Slices were then incubated with primary antibody overnight at 4ºC, followed by secondary antibody (1:600, Alexa Fluor, Invitrogen, Thermo Scientific or Jackson ImmunoResearch) incubation for 2 hours at room temperature and DAPI (Thermo Fisher, 62248, 1:50,000) staining for 10 min to counterstain nuclei. Thioflavin S (ThioS) staining was performed as previously described (Ly et al. 2011). Briefly, after incubation with secondary antibodies, brain slices were dehydrated and incubated with 1% ThioS (Sigma Aldrich, T1892) for 15 min. Slices were then rehydrated and washed in water. Brain slices were mounted with Fluoromount-G (Southern Biotech, 0100-01). The list of primary antibodies used are as follows: Aβ (6E10 clone, Biolegend, 803001, 1:1,000 or Novus Biologicals, NBP2-62566, 1:1,000), Bassoon (Synaptic Systems, 141016, 1:1000), DKK3 (R&D, AF948, 1:1,000), Gephyrin (Synaptic Systems, 147-002, 1:500), GFAP (Abcam, ab5541, 1:500), GFP (Millipore, 06-896, 1:500), Homer1 (Synaptic Systems, 160-003, 1:1,000), IBA1 (FUJIFILM Wako, 019-19741, 1:1,000), NeuN (Cell Signaling, 12943, 1:1,000), Neurofilament Heavy (Abcam, ab8135, 1:5,000), PSD-95 (Thermo Fisher Scientific, MA1-046, 1:500), vGAT (Synaptic Systems, 131-004, 1:500), vGLUT1 (Millipore, ab5905, 1:2,000), Wnt7a/b (R&D, AF3460, 1:1,000) and β-catenin (BD Biosciences, 610153, 1:1,000).

Image acquisition and analyses

Confocal images were acquired using a Leica SP8 microscope. For imaging plaque composition and synapses in the *stratum radiatum* region of the hippocampus, image stacks of 8 equidistant planes (240 nm, 76x76 nm/pixel) were obtained using a 63X (1.40 Numerical Aperture (NA) oil objective. For plaque quantification in the J20 brain, image stacks of 21 equidistant planes (50 nm) were obtained with a 20X (0.75 NA) objective. Analyses were performed using Volocity imaging software version 6.5.1 (Quorum Technologies) as previously described (Galli et al. 2014; Marzo et al. 2016).

Protein extraction and Western blot

Protein was extracted from WT and J20 hippocampi, primary hippocampal neurons or human hippocampus with RIPA buffer (10mM Tris, 100mM NaCl, 1mM EDTA, 1% Nonidet P-40, 0.1% SDS, 0.5% deoxycholate, pH = 8). Samples were then sonicated and centrifuged at 14,000g for 10 minutes at 4ºC. Supernatant representing the protein fraction (soluble) was collected. For human brain samples, the pellet was washed in RIPA buffer and solubilized in 4% SDS. Thereafter, samples were sonicated and centrifuged at 14,000g for 10 minutes at 4ºC to obtain the SDS-soluble fraction (insoluble protein fraction). Protein concentration was quantified using a BCA kit (Thermo Fisher Scientific) according to the manufacturer's protocol.

Protein extracts were resolved on 10% SDS-PAGE gels. PVDF membranes (GE Healthcare, GE10600021) were incubated with primary antibodies overnight at 4ºC, followed by incubation of secondary antibodies for 60 min at room temperature. The list of primary antibodies used are as follows: Aβ (6E10 clone, Biolegend, 803001, 1:1,000), DKK3 (R&D, AF948, 1:1,000), GAPDH (Abcam, ab181602, 1:5,000), GluA1 (Cell Signaling, 13185, 1:1,000), GluA1 phospho-Serine 845 (Cell Signaling, 8084, 1:1,000), Tubulin (Sigma, T9026, 1:5,000). The secondary antibodies conjugated with Horseradish Peroxidase (HRP) used were anti-goat IgG (Santa Cruz, sc-2020, 1:2,000 or R&D, HAF109, 1:10,000), anti-mouse IgG (GE Healthcare, NXA931, 1:3,000) and anti-rabbit IgG (GE Healthcare, NA934, 1:2,000). HRP-β-actin (Abcam, ab197277, 1:10,000) was incubated for 60min at room temperature. Chemiluminescent images were acquired using ChemiDoc (Image Lab, BioRad) and quantified by densitometric analysis using ImageJ-FIJI (NIH).

Behavioral tests

Two separate cohorts of 4-months old WT and J20 mice injected with Scr or DKK3 shRNA were used to perform behavioral tests. All tests were carried out in a dimly lit

room without noise interference. Animals were tracked using the automated SMART video tracking software (Panlab).

Elevated plus maze

Anxiety was tested using an elevated plus maze consisting of four arms (30.5x5cm each arm), two of which were surrounded by walls (enclosed arms). The apparatus was elevated 40 cm above the ground. Each mouse was placed in the central square (neutral area) facing an open arm, and time spent in the open and enclosed arms was measured for 5 min.

Open-field and Novel Object Location Test

Hippocampal-dependent spatial and recognition memory was tested using the Novel Object Location (NOL) test. The apparatus consisted of a square arena (45x45 cm), with cues in one of the walls. Mice were allowed to freely explore for 30 min to habituate them to the arena. Distance traveled and time spent in the center and in the periphery were measured. On the second day, two identical objects were placed equidistantly from walls and mice were allowed to explore for 10 min (NOL Acquisition). Twenty-four hours later, one of the objects was moved to a novel position and mice were allowed to explore for 5 min (NOL Testing). Object preference was measured as the percentage of time exploring the novel object location.

Morris Water Maze

Hippocampal-dependent spatial learning and memory was assessed using the Morris Water Maze (MWM) task as previously described (Marzo et al. 2016). In the first phase, mice performed four trials with a visible platform to check for deficiencies in vision or locomotion. The escape platform was made visible by using a high-contrast top surface and attaching a stripped flag. In the second phase, mice were trained to find a hidden platform with extra-maze visible cues for 6 days with 4 trials/day. The platform was submerged 2 cm below water and placed at the midpoint of one of the quadrants. Each mouse was allowed to search for the platform for up to 60 sec, after which mice that failed to reach the platform were placed on the platform. All mice were left on the platform for 10 sec before they were returned to their home cage. Probe trials were conducted before the fifth day of training (early probe) and 24h after the last day of training (late probe). During the probe trials, the platform was removed from the pool and mice were allowed to swim for 60 sec.

Statistical analyses

All graphed data are displayed as mean ± SEM. Statistical analyses were performed using GraphPad Prism version 8.0.2. Statistical outliers were determined using Grubbs and ROUT tests. Dataset normality was tested by the D'Agostino and Pearson or Shapiro-Wilk tests. When datasets passed normality, comparisons between two groups were analyzed using the unpaired two-sided Student's T-test whilst comparisons between more than two groups used one- or two- way ANOVA, followed by Tukey's multiple comparisons tests. For non-normally distributed data, comparisons between two groups were performed using the Mann-Whitney U test and comparisons between more than two groups with Kruskal-Wallis followed by Dunn's multiple comparison test. Pearson correlation coefficient was used for colocalization analyses. In all graphs, N-numbers corresponding to the number of independent primary cultures, animals, or human subjects, unless otherwise specified, are shown. In all figures, p-values are depicted as: *p-value≤0.05, **p-value≤0.01, ***p-value≤0.001.

REFERENCES

1000 Genomes Project Consortium et al., 2015. A global reference for human genetic variation. Nature, 526(7571), pp.68–74.

Abarzua, F. et al., 2005. Adenovirus-mediated overexpression of REIC/Dkk-3 selectively induces apoptosis in human prostate cancer cells through activation of c-Jun-NH2-kinase. Cancer Research, 65(21), pp.9617–9622.

Alarcón, M.A. et al., 2013. A novel functional low-density lipoprotein receptor-related protein 6 gene alternative splice variant is associated with Alzheimer's disease. Neurobiology of Aging, 34(6), pp.1709.e9–18.

Allen, M. et al., 2016. Human whole genome genotype and transcriptome data for Alzheimer's and other neurodegenerative diseases. Scientific data, 3, p.160089.

Barrantes, I. del B. et al., 2006. Generation and characterization of dickkopf3 mutant mice. Molecular and Cellular Biology, 26(6), pp.2317–2326.

Boughton, A.P. et al., 2021. LocusZoom.js: Interactive and embeddable visualization of genetic association study results. Bioinformatics, 37(18), pp.3017–3018.

Braak, H. et al., 2006. Staging of Alzheimer disease-associated neurofibrillary pathology using paraffin sections and immunocytochemistry. Acta Neuropathologica, 112(4), pp.389–404.

Bruggink, K.A. et al., 2015. Dickkopf-related protein 3 is a potential Aβ-associated protein in Alzheimer's Disease. Journal of Neurochemistry, 134(6), pp.1152–1162.

Caneparo, L. et al., 2007. Dickkopf-1 regulates gastrulation movements by coordinated modulation of Wnt/beta catenin and Wnt/PCP activities, through interaction with the Dally-like homolog Knypek. Genes & Development, 21(4), pp.465–480.

Caricasole, A. et al., 2003. Functional characterization of WNT7A signaling in PC12 cells: interaction with A FZD5 x LRP6 receptor complex and modulation by Dickkopf proteins. The Journal of Biological Chemistry, 278(39), pp.37024–37031.

Caricasole, A. et al., 2004. Induction of Dickkopf-1, a negative modulator of the Wnt pathway, is associated with neuronal degeneration in Alzheimer's brain. The Journal of Neuroscience, 24(26), pp.6021–6027.

Ciani, L. et al., 2011. Wnt7a signaling promotes dendritic spine growth and synaptic strength through Ca2+/Calmodulin-dependent protein kinase II. Proceedings of the National Academy of Sciences of the United States of America, 108(26), pp.10732–10737.

Clements, J.D. & Bekkers, J.M., 1997. Detection of spontaneous synaptic events with an optimally scaled template. Biophysical Journal, 73(1), pp.220–229.

De Ferrari, G.V. et al., 2007. Common genetic variation within the low-density lipoprotein receptor-related protein 6 and late-onset Alzheimer's disease. Proceedings of the National Academy of Sciences of the United States of America, 104(22), pp.9434–9439.

De Jager, P.L. et al., 2018. A multi-omic atlas of the human frontal cortex for aging and Alzheimer's disease research. Scientific data, 5, p.180142.

de Leeuw, C.A. et al., 2015. MAGMA: generalized gene-set analysis of GWAS data. PLoS Computational Biology, 11(4), p.e1004219.

DeLuca, D.S. et al., 2012. RNA-SeQC: RNA-seq metrics for quality control and process optimization. Bioinformatics, 28(11), pp.1530–1532.

Deuker, L. et al., 2014. Human neuroimaging studies on the hippocampal CA3 region - integrating evidence for pattern separation and completion. Frontiers in Cellular Neuroscience, 8, p.64.

Drummond, E. et al., 2017. Proteomic differences in amyloid plaques in rapidly progressive and sporadic Alzheimer's disease. Acta Neuropathologica, 133(6), pp.933–954.

Galli, S. et al., 2014. Deficient Wnt signalling triggers striatal synaptic degeneration and impaired motor behaviour in adult mice. Nature Communications, 5, p.4992.

Galli, S. et al., 2021. Striatal synapse degeneration and dysfunction are reversed by reactivation of wnt signaling. Frontiers in synaptic neuroscience, 13, p.670467.

Hesse, R. et al., 2019. Comparative profiling of the synaptic proteome from Alzheimer's disease patients with focus on the APOE genotype. Acta neuropathologica communications, 7(1), p.214.

Hong, S. et al., 2016. Complement and microglia mediate early synapse loss in Alzheimer mouse models. Science, 352(6286), pp.712–716.

Hu, N.-W. et al., 2009. GluN2B subunit-containing NMDA receptor antagonists prevent Abeta-mediated synaptic plasticity disruption in vivo. Proceedings of the National Academy of Sciences of the United States of America, 106(48), pp.20504–20509.

Kamal, A. et al., 1999. Chemical LTD in the CA1 field of the hippocampus from young and mature rats. The European Journal of Neuroscience, 11(10), pp.3512–3516.

Killick, R. et al., 2014. Clusterin regulates β-amyloid toxicity via Dickkopf-1-driven induction of the wnt-PCP-JNK pathway. Molecular Psychiatry, 19(1), pp.88–98.

Koffie, R.M. et al., 2012. Apolipoprotein E4 effects in Alzheimer's disease are mediated by synaptotoxic oligomeric amyloid-β. Brain: A Journal of Neurology, 135(Pt 7), pp.2155–2168.

Krenitsky, V.P. et al., 2012. Discovery of CC-930, an orally active anti-fibrotic JNK inhibitor. Bioorganic & Medicinal Chemistry Letters, 22(3), pp.1433–1438.

Krupnik, V.E. et al., 1999. Functional and structural diversity of the human Dickkopf gene family. Gene, 238(2), pp.301–313.

Kunkle, B.W. et al., 2019. Genetic meta-analysis of diagnosed Alzheimer's disease identifies new risk loci and implicates Aβ, tau, immunity and lipid processing. Nature Genetics, 51(3), pp.414–430.

Leroy, K., Yilmaz, Z. & Brion, J.P., 2007. Increased level of active GSK-3beta in Alzheimer's disease and accumulation in argyrophilic grains and in neurones at different stages of neurofibrillary degeneration. Neuropathology and Applied Neurobiology, 33(1), pp.43–55.

Li, S. et al., 2011. Soluble Aβ oligomers inhibit long-term potentiation through a mechanism involving excessive activation of extrasynaptic NR2B-containing NMDA receptors. The Journal of Neuroscience, 31(18), pp.6627–6638.

Liu, C.-C. et al., 2014. Deficiency in LRP6-mediated Wnt signaling contributes to synaptic abnormalities and amyloid pathology in Alzheimer's disease. Neuron, 84(1), pp.63–77.

Ly, P.T.T., Cai, F. & Song, W., 2011. Detection of neuritic plaques in Alzheimer's disease mouse model. Journal of Visualized Experiments, (53).

Marzo, A. et al., 2016. Reversal of synapse degeneration by restoring wnt signaling in the adult hippocampus. Current Biology, 26(19), pp.2551–2561.

McLeod, F. et al., 2018. Wnt Signaling Mediates LTP-Dependent Spine Plasticity and AMPAR Localization through Frizzled-7 Receptors. Cell reports, 23(4), pp.1060–1071.

McLeod, F. & Salinas, P.C., 2018. Wnt proteins as modulators of synaptic plasticity. Current Opinion in Neurobiology, 53, pp.90–95.

Meilandt, W.J. et al., 2009. Neprilysin overexpression inhibits plaque formation but fails to reduce pathogenic Abeta oligomers and associated cognitive deficits in human amyloid precursor protein transgenic mice. The Journal of Neuroscience, 29(7), pp.1977–1986.

Meister, M. et al., 2015. Dickkopf-3, a tissue-derived modulator of local T-cell responses. Frontiers in immunology, 6, p.78.

Mirra, S.S. et al., 1991. The Consortium to Establish a Registry for Alzheimer's Disease (CERAD). Part II. Standardization of the neuropathologic assessment of Alzheimer's disease. Neurology, 41(4), pp.479–486.

Mizobuchi, Y. et al., 2008. REIC/Dkk-3 induces cell death in human malignant glioma. Neuro-oncology, 10(3), pp.244–253.

Mucke, L., Yu, G.Q., et al., 2000. Astroglial expression of human alpha(1)-antichymotrypsin enhances alzheimer-like pathology in amyloid protein precursor transgenic mice. The American Journal of Pathology, 157(6), pp.2003–2010.

Mucke, L., Masliah, E., et al., 2000. High-level neuronal expression of abeta 1-42 in wild-type human amyloid protein precursor transgenic mice: synaptotoxicity without plaque formation. The Journal of Neuroscience, 20(11), pp.4050–4058.

Mucke, L. & Selkoe, D.J., 2012. Neurotoxicity of amyloid β-protein: synaptic and network dysfunction. Cold Spring Harbor perspectives in medicine, 2(7), p.a006338.

Niehrs, C., 2006. Function and biological roles of the Dickkopf family of Wnt modulators. Oncogene, 25(57), pp.7469–7481.

Niehrs, C., 2012. The complex world of WNT receptor signalling. Nature Reviews. Molecular Cell Biology, 13(12), pp.767–779.

Nusse, R. & Clevers, H., 2017. Wnt/β-Catenin Signaling, Disease, and Emerging Therapeutic Modalities. Cell, 169(6), pp.985–999.

Palomer, E. et al., 2022. Epigenetic repression of Wnt receptors in AD: a role for Sirtuin2-induced H4K16ac deacetylation of Frizzled1 and Frizzled7 promoters. Molecular Psychiatry. Published online ahead of print. Available from: 10.1038/s41380-022-01492-z.

Purro, S.A., Dickins, E.M. & Salinas, P.C., 2012. The secreted Wnt antagonist Dickkopf-1 is required for amyloid β-mediated synaptic loss. The Journal of Neuroscience, 32(10), pp.3492–3498.

Redlingshöfer, L. et al., 2020. Clathrin light chain diversity regulates membrane deformation in vitro and synaptic vesicle formation in vivo. Proceedings of the National Academy of Sciences of the United States of America, 117(38), pp.23527–23538.

Ring, D.B. et al., 2003. Selective glycogen synthase kinase 3 inhibitors potentiate insulin activation of glucose transport and utilization in vitro and in vivo. Diabetes, 52(3), pp.588–595.

Rosi, M.C. et al., 2010. Increased Dickkopf-1 expression in transgenic mouse models of neurodegenerative disease. Journal of Neurochemistry, 112(6), pp.1539–1551.

Ross, S.P. et al., 2018. miRNA-431 Prevents Amyloid-β-Induced Synapse Loss in Neuronal Cell Culture Model of Alzheimer's Disease by Silencing Kremen1. Frontiers in Cellular Neuroscience, 12, p.87.

Saito, T. et al., 2014. Single App knock-in mouse models of Alzheimer's disease. Nature Neuroscience, 17(5), pp.661–663.

Selkoe, D.J. & Hardy, J., 2016. The amyloid hypothesis of Alzheimer's disease at 25 years. EMBO Molecular Medicine, 8(6), pp.595–608.

Sellers, K.J. et al., 2018. Amyloid β synaptotoxicity is Wnt-PCP dependent and blocked by fasudil. Alzheimer's & Dementia, 14(3), pp.306–317.

Thompson, C.L. et al., 2008. Genomic anatomy of the hippocampus. Neuron, 60(6), pp.1010–1021.

Walsh, D.M. et al., 2002. Naturally secreted oligomers of amyloid beta protein potently inhibit hippocampal long-term potentiation in vivo. Nature, 416(6880), pp.535–539.

Wang, M. et al., 2018. The Mount Sinai cohort of large-scale genomic, transcriptomic and proteomic data in Alzheimer's disease. Scientific data, 5, p.180185.

Xiong, F., Ge, W. & Ma, C., 2019. Quantitative proteomics reveals distinct composition of amyloid plaques in Alzheimer's disease. Alzheimer's & Dementia, 15(3), pp.429–440.

Xu, J. et al., 2019. Regional protein expression in human Alzheimer's brain correlates with disease severity. Communications Biology, 2, p.43.

Ye, C. et al., 2004. Amyloid beta-protein induced electrophysiological changes are dependent on aggregation state: N-methyl-D-aspartate (NMDA) versus non-NMDA receptor/channel activation. Neuroscience Letters, 366(3), pp.320–325.

Yu, B. et al., 2017. A Cytokine-Like Protein Dickkopf-Related Protein 3 Is Atheroprotective. Circulation, 136(11), pp.1022–1036.

Zenzmaier, C. et al., 2009. Dkk-3 is elevated in CSF and plasma of Alzheimer's disease patients. Journal of Neurochemistry, 110(2), pp.653–661.

Zhang, J. et al., 2015. A WNT1-regulated developmental gene cascade prevents dopaminergic neurodegeneration in adult En1(+/-) mice. Neurobiology of Disease, 82, pp.32–45.

Zhang, Li et al., 2017. Dickkopf 3 (Dkk3) Improves Amyloid-β Pathology, Cognitive Dysfunction, and Cerebral Glucose Metabolism in a Transgenic Mouse Model of Alzheimer's Disease. Journal of Alzheimer's Disease, 60(2), pp.733–746.

Zhang, Y. et al., 2014. An RNA-sequencing transcriptome and splicing database of glia, neurons, and vascular cells of the cerebral cortex. The Journal of Neuroscience, 34(36), pp.11929–11947.

Zhu, Y. et al., 2014. Phosphatase WIP1 regulates adult neurogenesis and WNT signaling during aging. The Journal of Clinical Investigation, 124(7), pp.3263–3273.

FIGURES

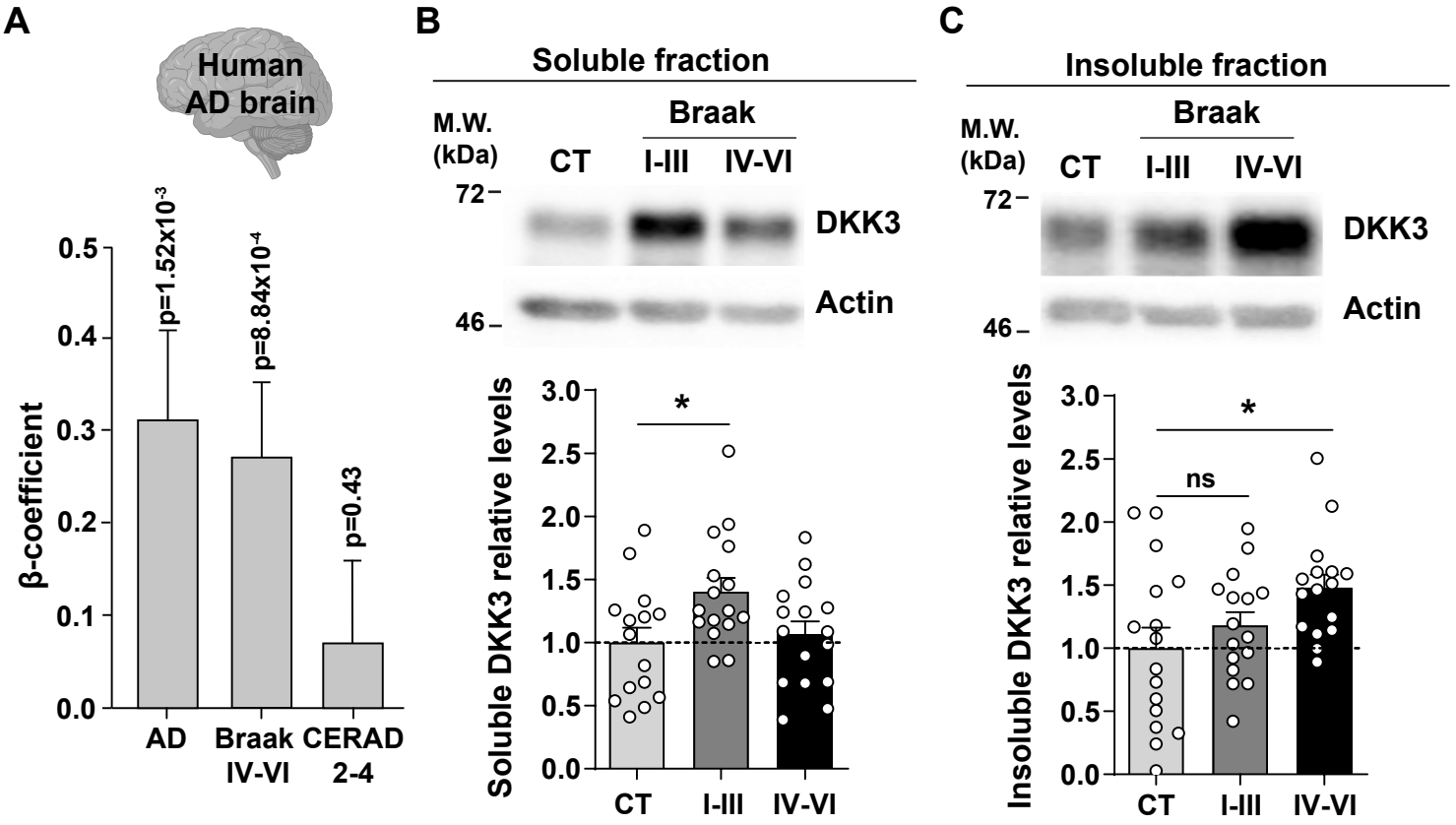

Figure 1

Figure 1. DKK3 mRNA and protein levels are increased in the human AD brain.

(**A**) Temporal cortex RNAseq dataset logistic regression shows that *DKK3* mRNA levels are increased in AD cases relative to controls. Ordinal regression shows that *DKK3* is differentially expressed for Braak scores IV-VI but not for CERAD scores 2-4.

(**B, C**) Representative immunoblots of DKK3 and loading control actin in (**B**) soluble and (**C**) insoluble protein fractions from the hippocampus of control (CT; n = 15-16), Braak stages I-III (n = 16) and Braak stage IV-VI (n = 16) individuals (One-Way ANOVA test followed by Tukey's multiple comparisons). See also **Table S1**.

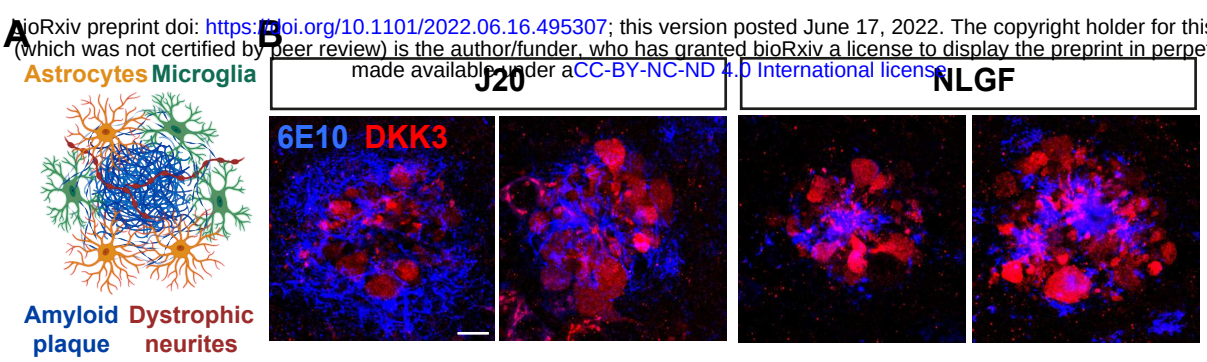

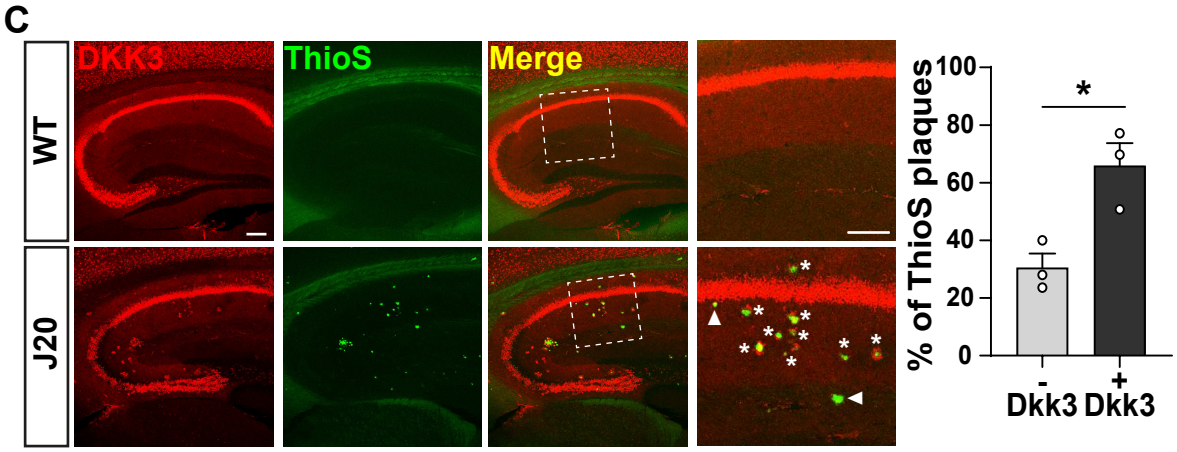

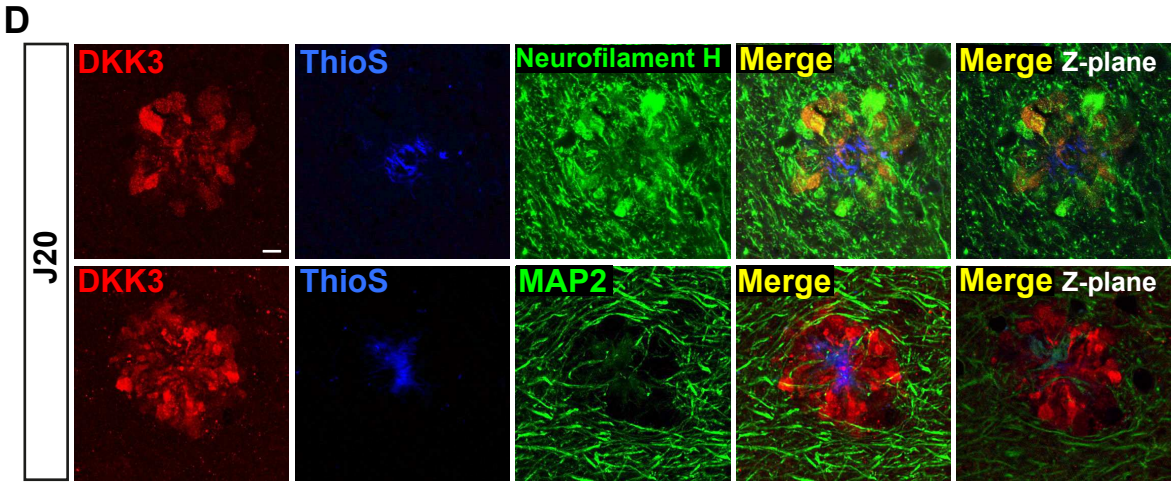

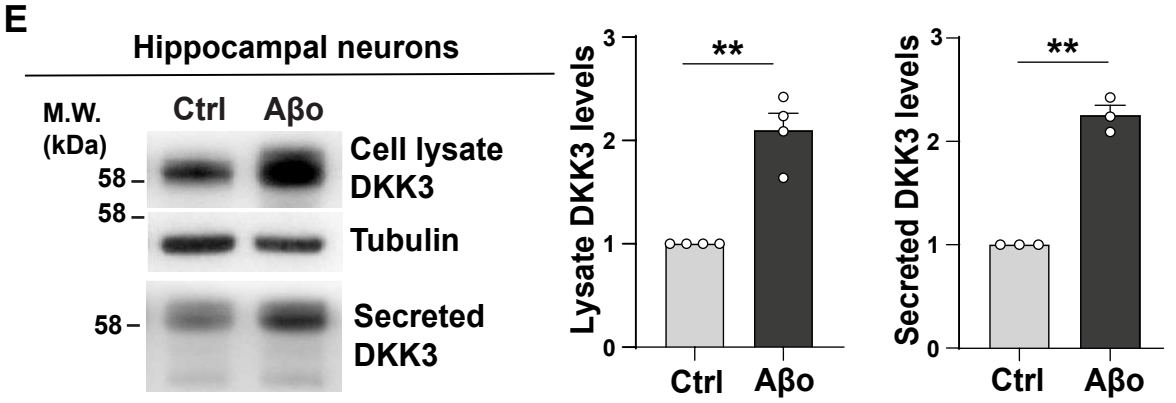

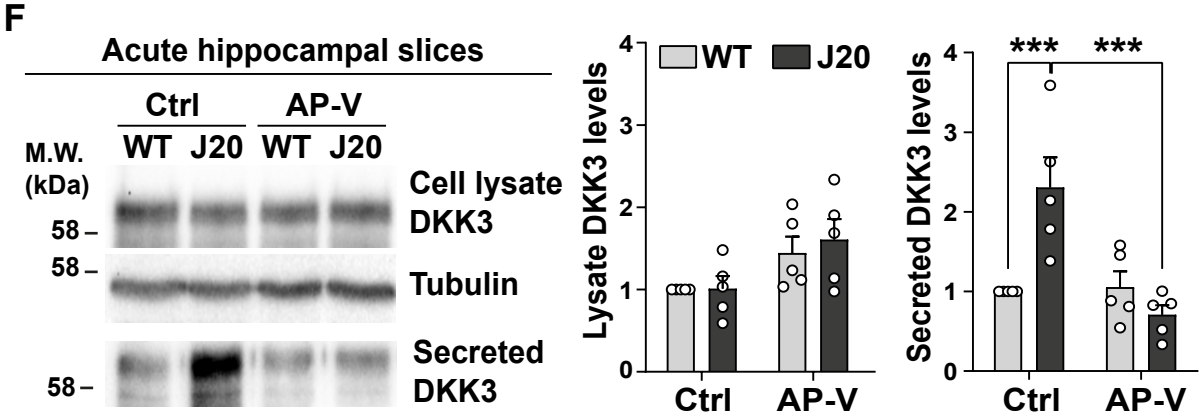

Figure 2

Figure 2. DKK3 localizes to dystrophic neurites around Aβ plaques, and its secretion is increased by Aβo and in the brain of J20 AD mouse model.

(**A**) Diagram of the components of an Aβ plaque (blue), astrocytes (orange), microglia (green), and dystrophic neurites (red).

(**B**) Confocal images of DKK3 protein (red) and amyloid plaques stained with the 6E10 antibody (blue) in the hippocampus of 18-months old J20 and 8-months NLGF mice. Scale bar = 10μm. See also **Figure S1**.

(**C**) Confocal images of DKK3 (red) and Aβ plaques labeled by Thioflavin S (ThioS; green) in the hippocampus of 18-months old WT and J20 mice. ThioS+ plaques not containing DKK3 (- DKK3; arrowheads), ThioS+ plaques containing DKK3 (+ DKK3; asterisks). Scale bar = 140μm and 100 μm in zoom-in pictures. Graph depicts quantification of the percentage of ThioS+ plaques containing DKK3 (Student's T-test, n = 3 animals per genotype). See also **Figure S2A**.

(**D**) Z-stack confocal images show that DKK3 (red) accumulates at Aβ plaques (ThioS; blue) and colocalizes with atrophic axons (Neurofilament-H; green) but not with dendrites (MAP2; green). XY views of one plane are shown in the last panel. Scale bar = 6μm. See also **Figure S2B&C**.

(E) Representative immunoblot shows DKK3 levels in the lysate and in the extracellular media (secreted DKK3) of cultured hippocampal neurons treated with vehicle (Ctrl) or Aβo. Tubulin was used as loading control in cell lysates. Graphs show densiometric quantifications relative to control (Student's T-test; n = 3 independent experiments). See also **Figure S3A**.

(**F**) Immunoblot images show DKK3 levels in the cell lysate and secreted fraction of acute hippocampal slices of 3-4-months old WT and J20 mice. Slices were incubated with vehicle (Ctrl) or APV for 3 hours. Tubulin was used as loading control in the homogenate. Graphs show densiometric quantifications relative to control (Two-Way ANOVA followed by Tukey's post-hoc test; n = 5 animals). See also **Figure S3C,D&E**.

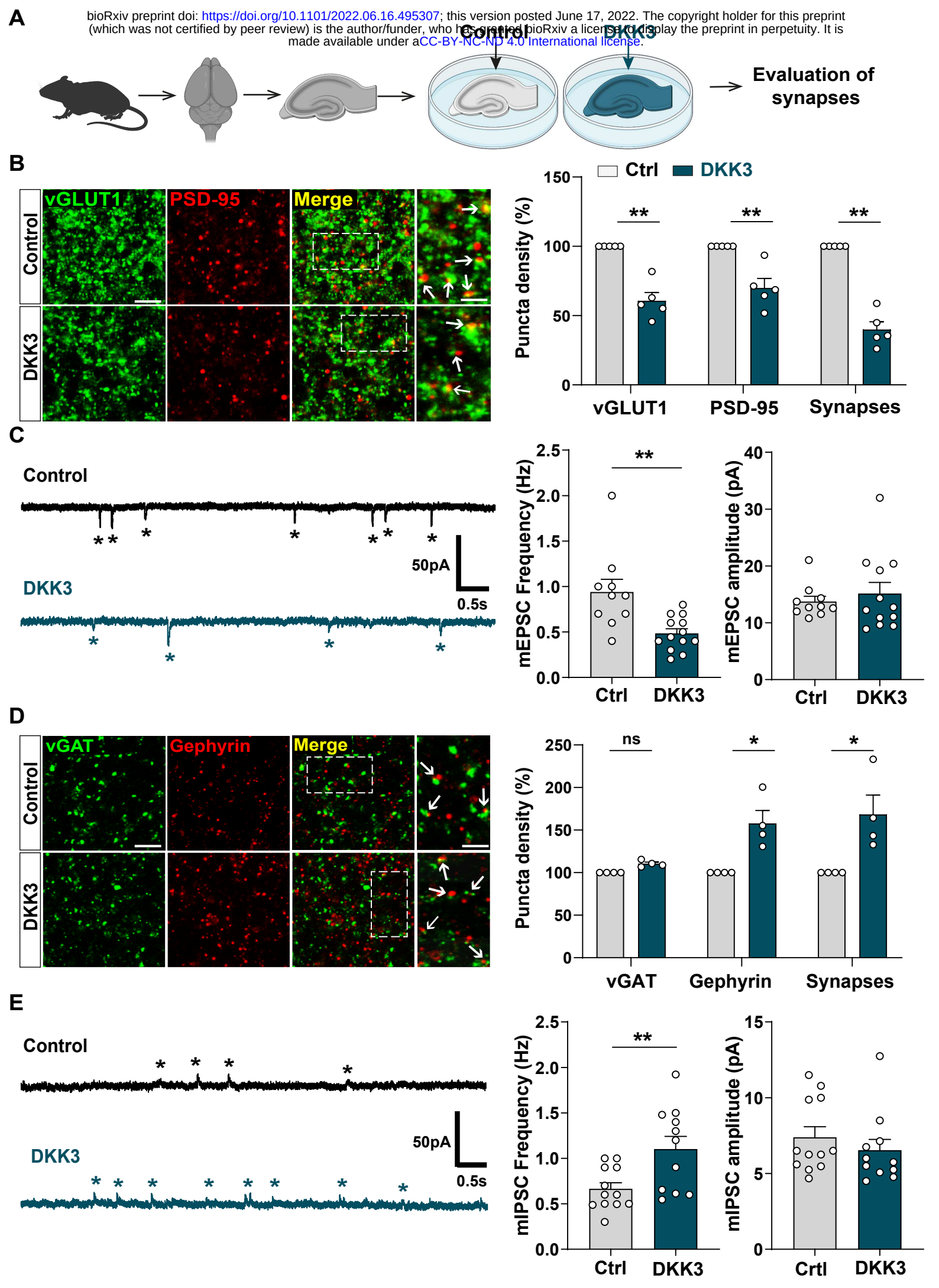

Figure 3

Figure 3. Gain-of-function of DKK3 leads to opposing effects on the number of excitatory and inhibitory synapses in the hippocampus.

(**A**) Diagram depicting the treatment of hippocampal brain slices obtained from 3-months old adult WT mice with vehicle (Ctrl) or recombinant DKK3 protein. Synapses were evaluated by confocal microscopy and electrophysiological recordings. See also **Figure S4A&B**.

(**B**) Confocal images of the CA3 SR region labeled with the presynaptic excitatory marker vGLUT1 (green) and the postsynaptic marker PSD-95 (red). Arrows indicate excitatory synapses. Scale bar = 5µm and 2.5µm in zoomed-in pictures. Quantification is shown on the right-hand side (Mann-Whitney test, n = 5 animals per condition). See also **Figure S4C**.

(**C**) Representative mEPSC traces recorded at -60mV from CA3 cells. Stars indicate mEPSC events. Quantification of mEPSC frequency and amplitude are shown on the right-hand side (Mann-Whitney test, n = 10-13 cells from 5 animals).

(**D**) Confocal images of the CA3 SR region labeled with the presynaptic inhibitory marker vGAT (green) and the postsynaptic marker gephyrin (red). Arrows indicate inhibitory synapses. Scale bar = 5µm and 2.5µm in zoomed-in pictures. Quantification is shown on the right-hand side (Mann-Whitney test, n = 4 animals per condition). See also **Figure S4D**.

(**E**) Representative mIPSC traces recorded at 0mV from CA3 cells. Stars indicate mIPSC events. Quantification of mIPSC frequency and amplitude are shown on the right-hand side (Student's T-test for mIPSC frequency and Mann-Whitney test for mIPSC amplitude, n = 11-12 cells from 5-7 animals).

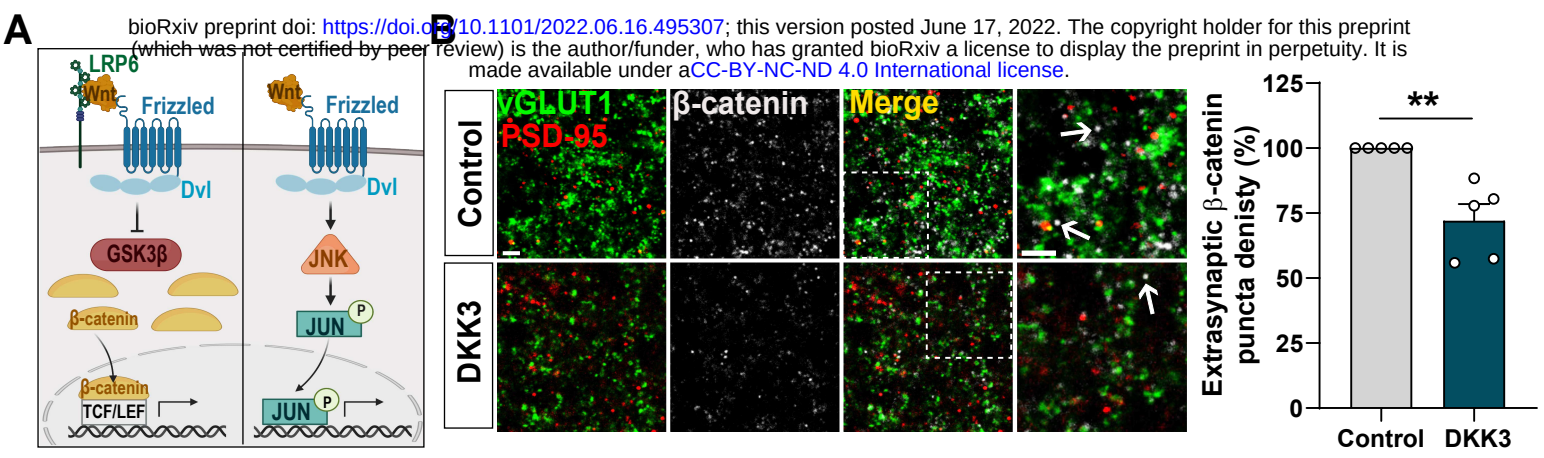

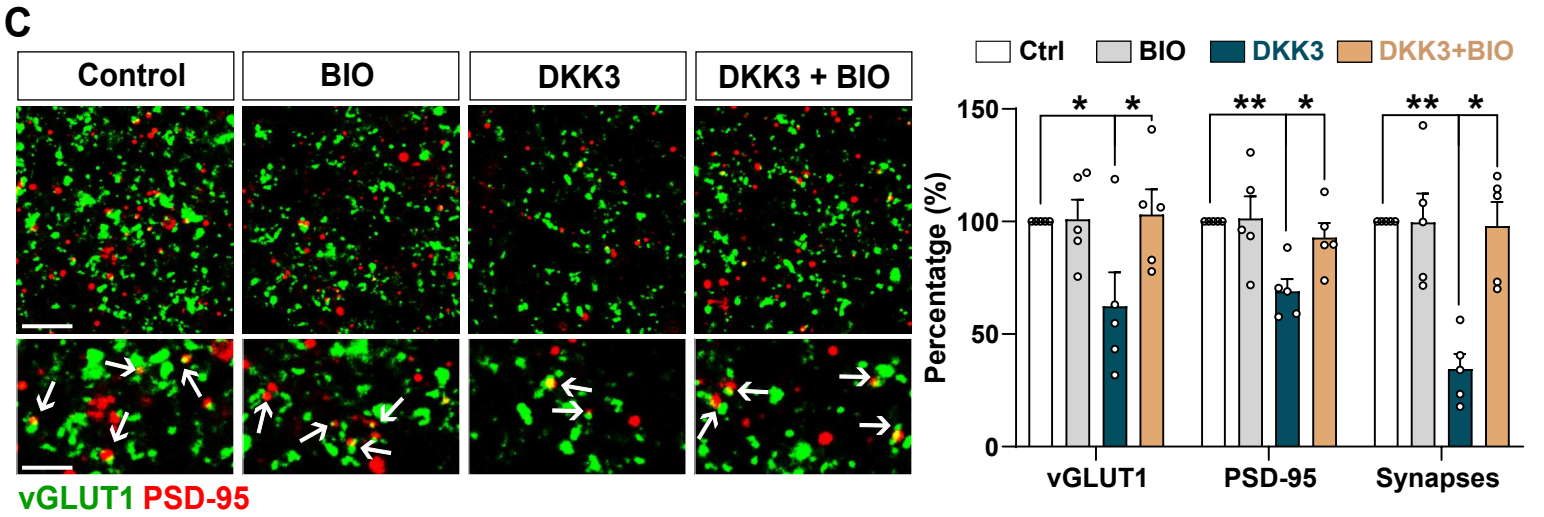

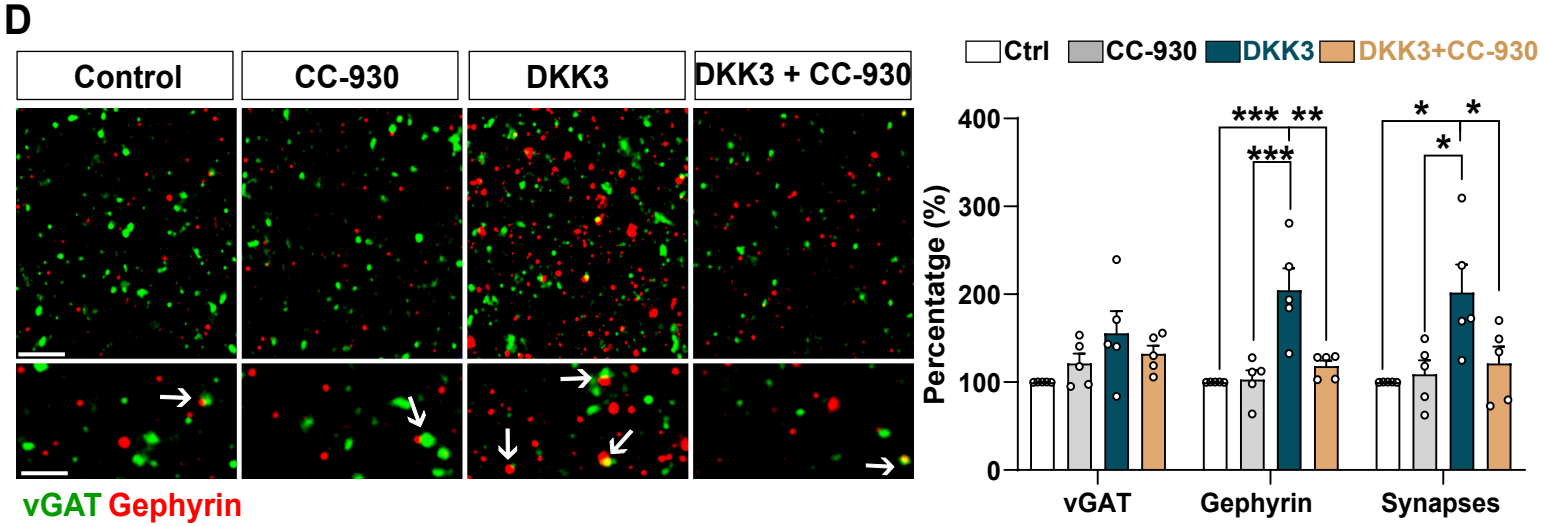

Figure 4

Figure 4. DKK3 regulates excitatory and inhibitory synapse number through the Wnt/GSK3β and Wnt/JNK pathways respectively. See also **Figure S4E&F**.

(**A**) Diagram of the Wnt pathways signaling through GSK3β (left: Wnt/GSK3β pathway) or JNK (right: Wnt/JNK pathway).

(**B**) Confocal images show excitatory synapses, visualized by colocalization of vGLUT1 (green) and PSD-95 (red), and β-catenin puncta (grey) in the CA3 SR. Arrows indicate extra-synaptic β-catenin puncta. Scale bar = 2.5μm. Quantification of extrasynaptic β-catenin puncta density as a percentage of control is shown on the right-hand side (Mann-Whitney test, n = 5 animals).

(**C**) Confocal images show excitatory synapses (co-localized vGLUT1 in green and PSD-95 in red) in the CA3 SR after treatment with vehicle (Ctrl) or DKK3 in the absence or presence of BIO for 4h. Scale bar = 5μm and 2.5μm. Graph shows the quantification of puncta density as a percentage of control (Kruskal-Wallis followed by Dunn's multiple comparisons, n = 5 animals).

(**D**) Confocal images showing inhibitory synapses defined by the colocalization of vGAT (green) and gephyrin (red) in the CA3 SR after treatment with vehicle (Ctrl) or DKK3 in the absence or presence of CC-930 for 4h. Scale bar = 5μm and 2.5μm. Graph shows the quantification of puncta density as a percentage of control (Kruskal-Wallis followed by Dunn's multiple comparisons, n = 5 animals).

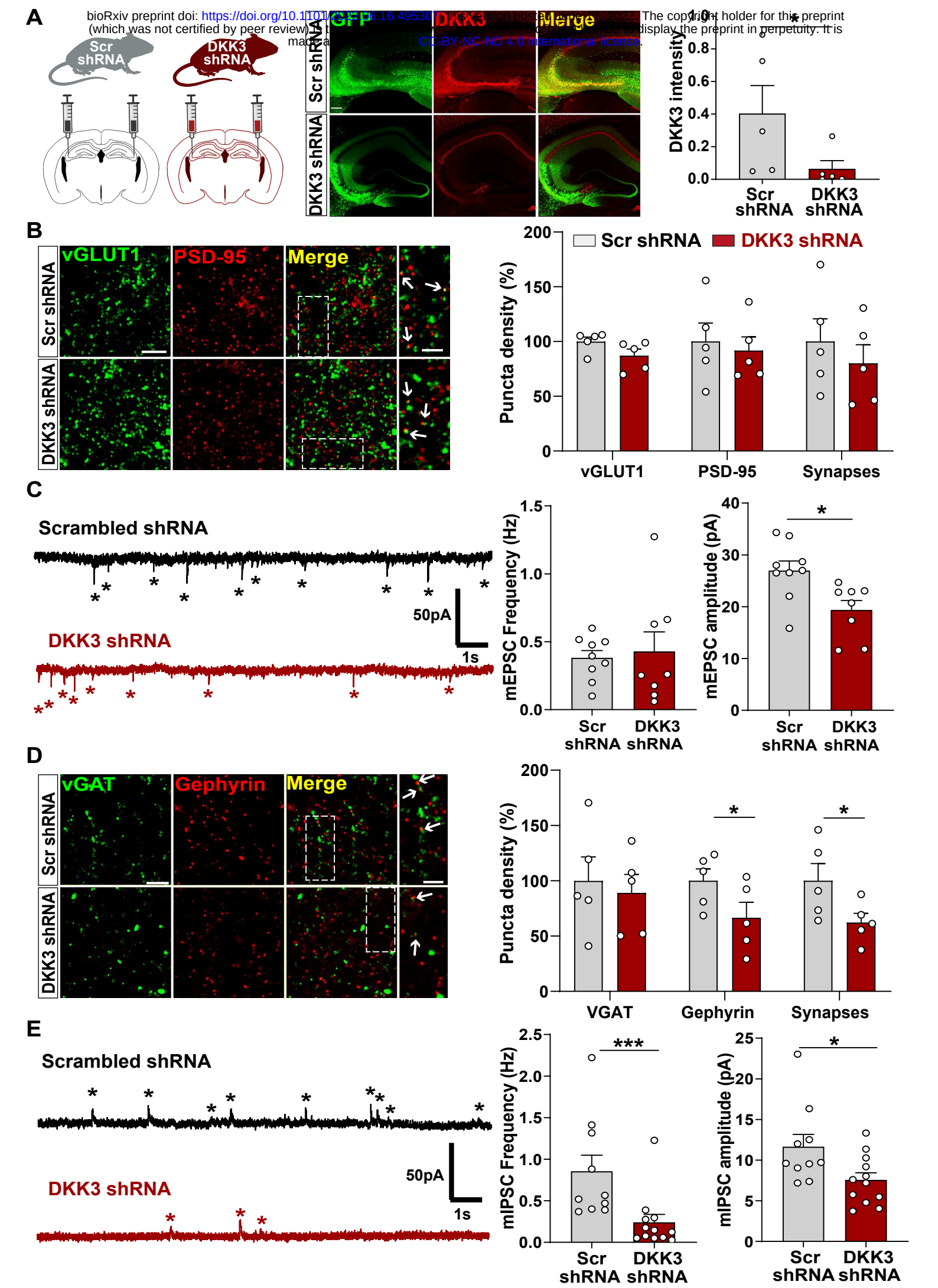

Figure 5

Figure 5. *In vivo* loss-of-function of DKK3 decreases inhibitory synapses but does not affect excitatory synapses in the hippocampus.

(**A**) Diagram showing the experimental design. 3-months old WT mice were injected with AAV9 scrambled (Scr) or DKK3 shRNA in the CA3 region. Confocal images showing GFP (green) and DKK3 (red) in Scr- and DKK3-shRNA injected hippocampus. Scale bar = 145μm. Graph shows quantification of DKK3 intensity in the area injected with the viruses.

(**B**) Confocal images from hippocampal CA3 SR show excitatory synapses (colocalized vGLUT1 in green and PSD-95 in red). Arrows indicate excitatory synapses. Scale bar = 5μm and 2.5μm in zoomed-in images. Quantification is shown on the right-hand side (Student's T-test, n = 5 animals per condition).

C) Representative mEPSC traces recorded at -60mV from CA3 cells. Stars indicate mEPSC events. Quantification of mEPSC frequency and amplitude are shown on the right-hand side (Student's T-test, n = 8-9 cells from 4 animals).

(**D**) Confocal images from hippocampal CA3 SR show inhibitory synapses (colocalized vGAT in green and gephyrin in red). Arrows point to inhibitory synapses. Scale bar = 5μm and 2.5μm in zoomed-in pictures. Quantification is shown on the right-hand side (Student's T-test, n = 5 animals).

(**E**) Representative mIPSC traces recorded at 0mV from CA3 cells. Stars indicate mIPSC events. Quantification of mIPSC frequency and amplitude are shown on the right-hand side (Mann-Whitney test, n = 10-12 cells from 6 animals).

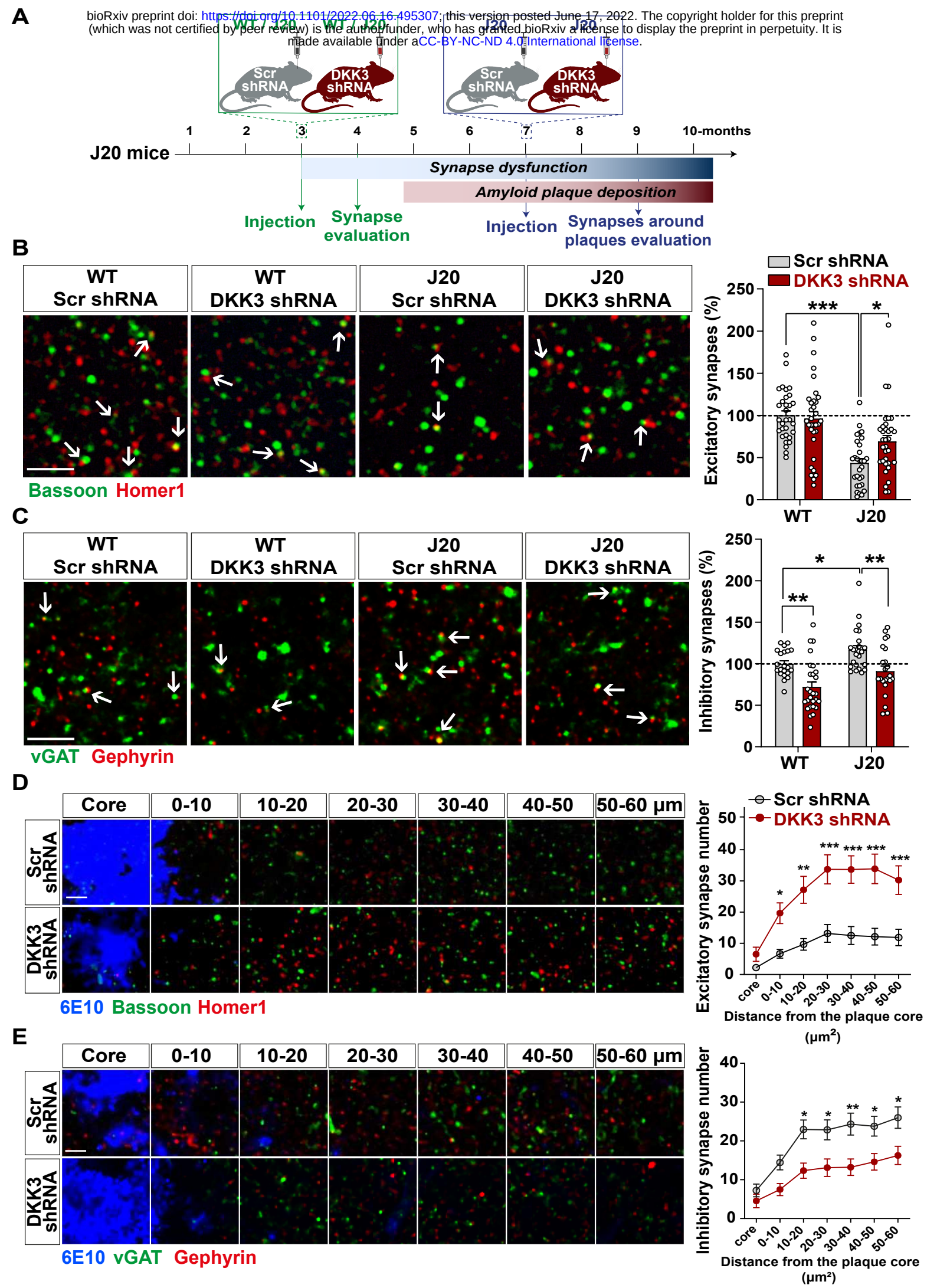

Figure 6

Figure 6. *In vivo* loss-of-function of DKK3 rescues synaptic changes in the hippocampus of J20 mice before and after Aβ plaque formation.

(**A**) Diagram depicting the experimental design. In green, 3-months old WT and J20 mice were injected bilaterally with AAV9-Scr shRNA or AAV9-DKK3 shRNA in the CA3 region. Density of synapses was evaluated at 4-months old, before plaque deposition starts. In blue, 7-months old J20 mice were injected bilaterally with AAV9-Scr shRNA or AAV9-DKK3 shRNA in the CA3 region. The density of synapses around plaques was evaluated at 9-months old. See also **Figure S5A**.

(**B, C**) Representative confocal images from the CA3 SR region of 4-months old WT and J20 mice. Images show (**B**) excitatory synapses (Bassoon in green and Homer1 in red) and (**C**) inhibitory synapses (vGAT in green and Gephyrin in red). Arrows point to synapses. Scale bar = 2.5µm. Quantification of synapse number as a percentage relative to WT-Scr shRNA animals is shown on the right-hand side (Two-Way ANOVA followed by Tukey's post-hoc test, n = 9-11 animals per condition and 2-3 brain slices per animal). See also **Figure S5B&C**.

(**D, E**) Representative confocal images from the CA3 SR region of 9-months old J20 mice. Images show an Aβ plaque (6E10; blue) and (**D**) excitatory synapses (Bassoon in green and Homer1 in red) or (**C**) inhibitory synapses (vGAT in green and Gephyrin in red) at different distances relative to the core of the plaque. Scale bar = 2.5µm. Graphs show synapse number per 200µm^3 at each distance (Two-Way ANOVA followed by Tukey's post-hoc test, n = 6-7 animals per condition and 2-3 brain slices per animal). See also **Figure S5D&E**.

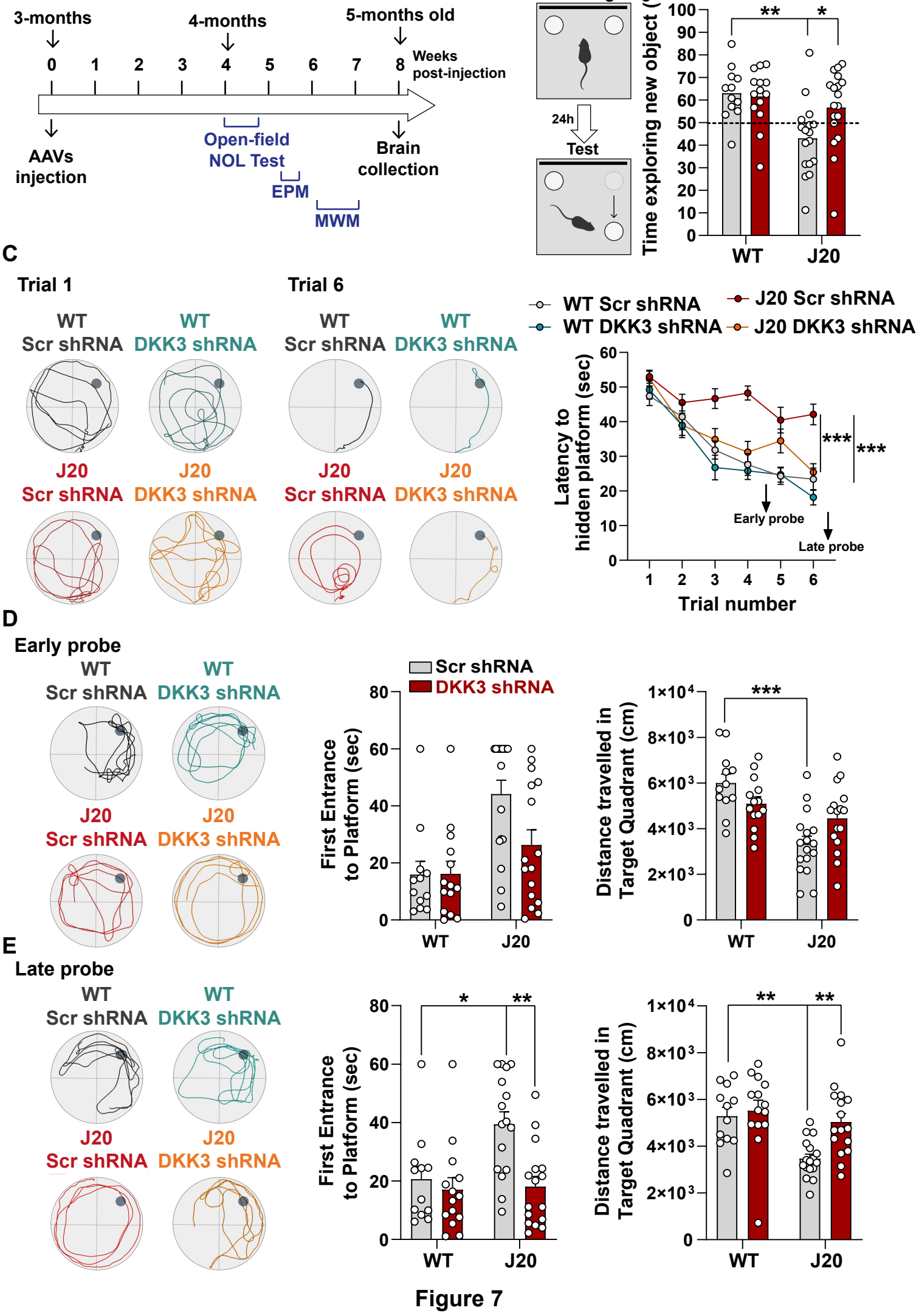

Figure 7

Figure 7. *In vivo* loss-of-function of DKK3 improves spatial memory in J20 mice. See also **Figure S6**.

(**A**) Diagram depicting that 3-months old WT and J20 mice were injected bilaterally with AAV9-Scr shRNA or AAV9-DKK3 shRNA in the CA3 area of the hippocampus. One month later, the behavior of animals was assessed using the Open-field, Novel Object Location (NOL) test, Elevated-Plus Maze (EPM) and the Morris water maze (MWM). See also **Figure S6A&B**.

(**B**) Novel Object Location Test. The percentage of time exploring the new object location *versus* the total time was evaluated (Two-Way ANOVA with Tukey's post-hoc test, n = 12 WT Scr shRNA, 14 WT DKK3 shRNA, 17 J20 Scr shRNA, 16 J20 DKK3 shRNA).

(**C- E**) Morris Water Maze. See also **Figure S6C**.

(**C**) Representative traces for the MWM Trials 1 and 6 are shown. Graph on the right shows the escape latency. Two-way ANOVA with repeated measures showed a significant effect over trials (animal group $F_{(3,55)} = 16.97$, p-value<0.0001; trial $F_{(5,259)} = 42.94$, p-value = 0.457; animal group and trial interaction $F_{(15,275)} = 2.753$, p-value = 0.0006). For all analyses (n=12 WT Scr shRNA, 14 WT DKK3 shRNA, 17 J20 Scr shRNA, 16 J20 DKK3 shRNA). Graph show comparison between groups (Two-way ANOVA followed by Tukey's multiple comparisons).

(**D, E**) Representative traces for the (**D**) Early and (**E**) Late probes. Graphs on the right show the time (sec) to first reach the target location (Kruskal Wallis followed by Dunns' multiple comparisons) and the distance (cm) traveled in the target quadrant (Two-way ANOVA followed by Tukey's post-hoc test for the early trial or Kruskal Wallis followed by Dunns' multiple comparisons).

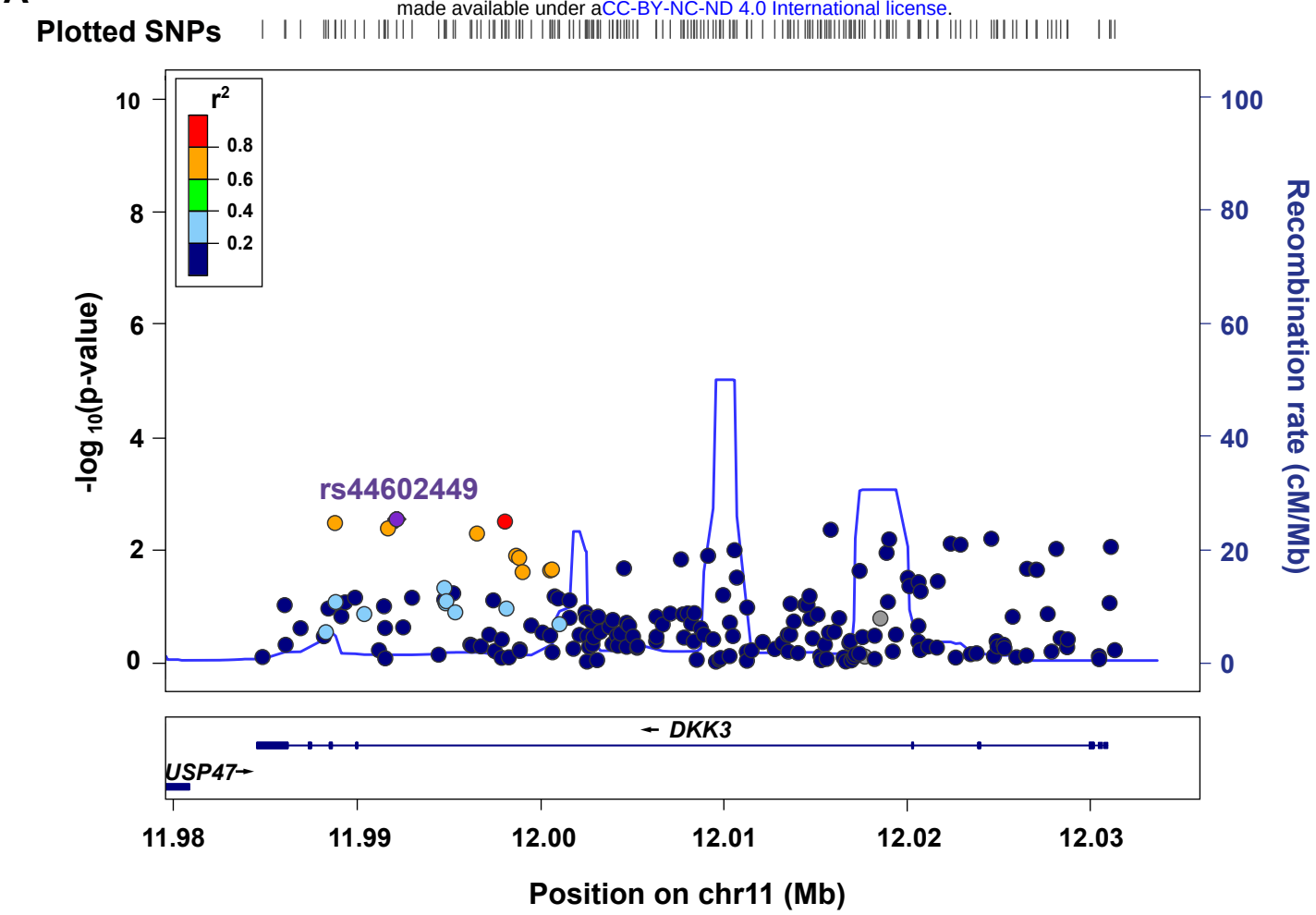

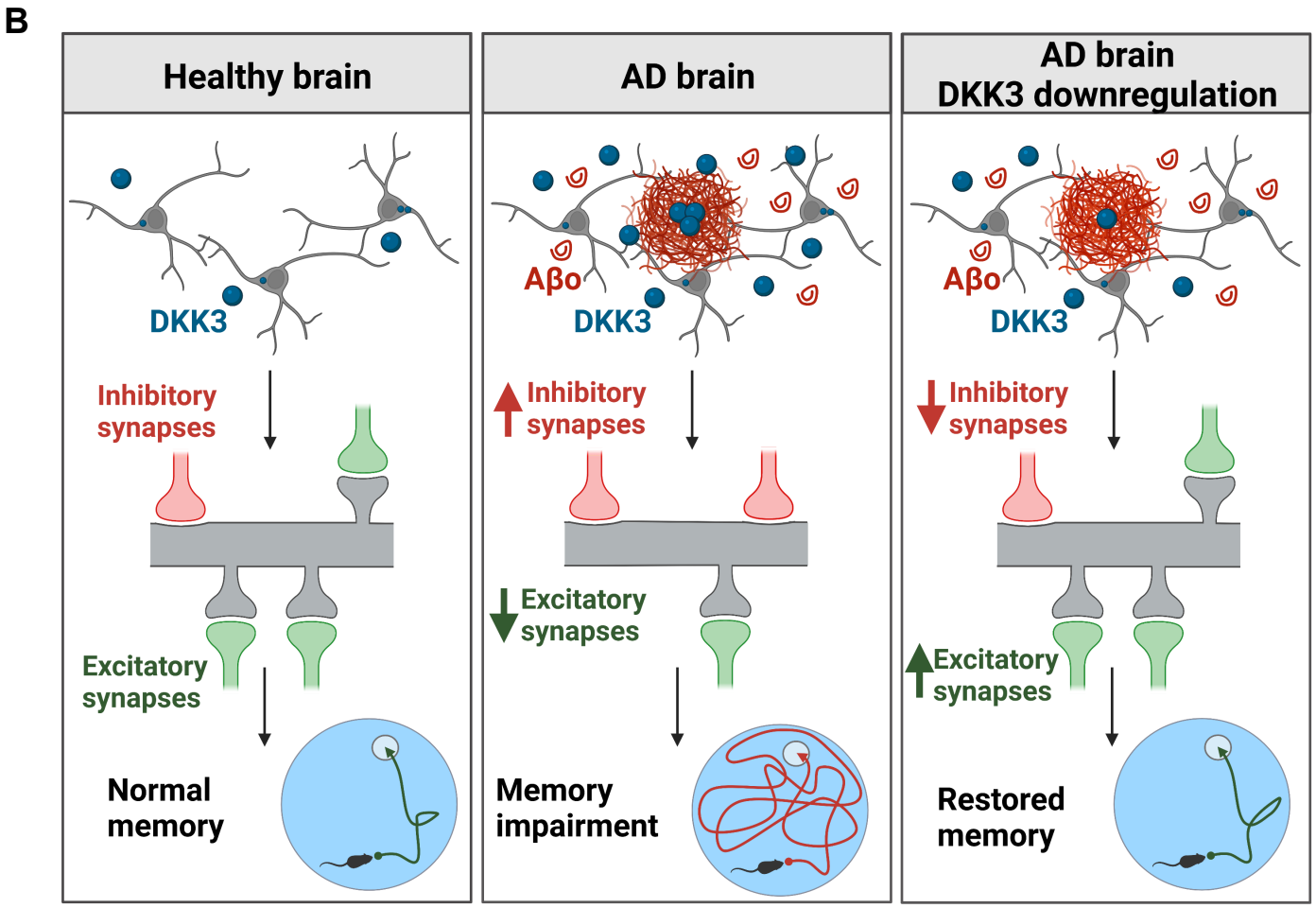

Figure 8

Figure 8. *DKK3* is genetically associated with late-onset AD.

(**A**) Individual *DKK3*-SNPs' association with late-onset AD was examined using AD summary statistics (Kunkle et al. 2019). 211 SNPs (plotted on top of the graph) were included in the analysis. SNPs are plotted as circles. The color of each circle reflects the degree of linkage disequilibrium (r^2) with the key SNP (rs11602449; purple diamond). See also **Table S2**.

(**B**) Proposed model of DKK3 function in the healthy and AD brain. In the adult healthy brain, DKK3 regulates the maintenance of both excitatory and inhibitory synapses in the hippocampus, leading to normal cognitive function. In the AD brain, DKK3 secretion is increased and later accumulates in Aβ plaques, inducing changes in excitatory and inhibitory synapses and triggering memory impairment. Downregulation of DKK3 restores synapse number and hippocampal-mediated memory in AD.